bioRxiv preprint doi: https://doi.org/10.1101/2020.09.01.277764; this version posted September 1, 2020. The copyright holder for this preprint (which was not certified by peer review) is the author/funder. All rights reserved. No reuse allowed without permission.

Rabaptin5 targets autophagy to damaged early endosomes and Salmonella containing vacuoles by interaction with FIP200 and ATG16L1

Valentina Millarte, Simon Schlienger, Simone Kälin, and Martin Spiess*

Biozentrum, University of Basel, Klingelbergstrasse 70, CH-4056 Basel, Switzerland

*Corresponding author: martin.spiess@unibas.ch
ORCID Spiess M: https://orcid.org/0000-0001-7139-0550

Summary

Selective autophagy of damaged organelles is an important process for cellular homeostasis. The mechanisms how autophagy selects specific targets is often poorly understood. Rabaptin5 was previously known as a major regulator of early endosome identity and maturation. Here we identified two novel Rabaptin5 interactors: FIP200, a subunit of the ULK1 autophagy initiator complex, and ATG16L1, a central component of the E3-like enzyme in LC3 lipidation. Indeed, autophagy of early endosomes damaged by chloroquine or monensin treatment was found to require Rabaptin5 and particularly a specific short sequence motif binding to the WD domain of ATG16L1. Rabaptin5 and this interaction with ATG16L1 is further required for much of autophagic elimination of *Salmonella enterica* in phagosomes with early endosomal characteristics early after infection. Our results demonstrate a novel function of Rabaptin5 in quality control of early endosomes as a selective receptor to recruit autophagy to damaged early endosomes and phagosomes.

Keywords: Autophagy, Rabaptin5, FIP200, ATG16L1, early endosomes, phagophores

bioRxiv preprint doi: https://doi.org/10.1101/2020.09.01.277764; this version posted September 1, 2020. The copyright holder for this preprint (which was not certified by peer review) is the author/funder. All rights reserved. No reuse allowed without permission.

INTRODUCTION

Autophagy is a self-degradative survival mechanism of eukaryotic cells important to preserve cellular homeostasis in response to stress conditions such as lack of nutrients, accumulation of misfolded or aggregated proteins, damaged organelles, and pathogen infection (Bento et al., 2016; Dikic and Elazar, 2018; Mercer et al., 2018; Morishita and Mizushima, 2019). Clearance of damaged organelles is an important process to preserve overall organelle function. Defects in its mechanisms have been shown to contribute to some forms of cancer, to neurodegeneration, and inflammatory diseases (Anding and Baehrecke, 2017; Leidal et al., 2018). Selective autophagy has been described for many organelles including mitochondria, peroxisomes, endoplasmic reticulum, and lysosomes (mitophagy, pexophagy, ER-phagy, and lysophagy; Kirkin and Rogov, 2019).

In the best studied case of starvation, autophagy is set in motion by activation of the ULK1–FIP200–ATG13–ATG101 initiator complex under the control of mTOR (mammalian target of rapamycin). The ULK1 complex initiates a dynamic interactome of components for the biogenesis of autophagosomes. It recruits and activates the class III phosphatidylinositol (PI) 3-kinase complex VPS34–VPS15–Beclin1–ATG14 on the nascent cup-shaped double-membrane phagophore initially derived from the endoplasmic reticulum or recycling endosomes. VPS34 produces PI-3-phosphate (PI3P) to recruit PI3P-binding proteins, such as WIPI (WD-repeat phosphoinositide interacting protein) family members important to acquire membranes of various origins. Together, these complexes and PI3P bind ATG16L1 with its partners ATG12–ATG5 to act as an E3-ubiquitin ligase-like enzyme for the lipidation of ubiquitin-like LC3 family proteins LC3A–C or GABARAP pre-activated by an LC3 conjugation system. LC3 proteins are required for elongation and closure of the phagophore membrane, before fusion with lysosomes.

Selective autophagy of protein aggregates or organelles destined for degradation differs from starvation-induced autophagy of cytosol (1) in autophagy inititation, which is independent of the nutrient situation and thus of regulation by mTOR and ULK1, and (2) in requiring a mechanism of targeting phagophores to the specific cargo (Kirkin and Rogov, 2019). A common feature of many autophagy targets is poly-ubiquitination, e.g. of misfolded proteins in aggregates or – in the case of damaged organelles or invading bacteria – of proteins not normally exposed to the cytosol. Selective autophagy receptors (SARs), such as p62/SQSTM1, optineurin, and NDP52, recognize ubiquitin on target structures and bind via specific LC3-interacting regions (LIRs) to LC3 on the phagophores (Johansen and Lamark, 2019; Kirkin and Rogov, 2019; Morishita and Mizushima, 2019). Furthermore, ubiquitin on damaged endomembranes is also directly recognized by ATG16L1, a core component of the LC3 lipidation complex (Fujita et al., 2013). ATG16L1 emerges as an important hub for specific cargo to connect to the autophagy machinery. It forms a complex with ATG5 and ATG12 for LC3 lipidation and has binding sites for FIP200 and WIPI2 (Dooley et al., 2014; Gammoh et al., 2013), for phosphoinositides (Dudley et al., 2019) and generally for membranes (Lystad et al., 2019). On the other hand, it was shown to interact with TRIM16, an E3 ubiquitin ligase required for autophagy of damaged lysosomes by connecting to galectin3 on exposed glycans (Chauhan et al., 2016), and with TMEM59 involved in autophagic degradation of late endosomes/lysosomes and *Staphylococcus aureus*-containing phagosomes (Boada-Romero et al., 2013).

As to the initiation of selective autophagy, recent studies demonstrated also a connection between SARs and FIP200 of the initiator complex. FIP200 binds directly to p62 in a segment that also includes the LIR (Turco et al., 2019). LC3 binding to the LIR displaces FIP200 from p62, suggesting an attractive mechanism of progression from autophagy initiation to phagophore engulfment. Similarly, NDP52 was demonstrated to bind FIP200 facilitated by the kinase TBK1 (Vargas et al., 2019), supporting the concept that SARs recruited to ubiquitinated damaged organelles locally initiate autophagosome biogenesis by interaction with the ULK1/FIP200 complex.

Besides the mechanisms of autophagy described above where a double-membrane phagophore is produced to engulf the target for subsequent fusion to lysosomes, noncanonical autophagy or LC3-associated phagocytosis (LAP) as well as LC3-associated endocytosis (LANDO) of β-amyloid have been described as a process in which the LC3 conjugation system including the ATG16L1–ATG5–ATG12 complex is recruited directly to a single-

bioRxiv preprint doi: https://doi.org/10.1101/2020.09.01.277764; this version posted September 1, 2020. The copyright holder for this preprint (which was not certified by peer review) is the author/funder. All rights reserved. No reuse allowed without permission.

membrane phagosome for fusion with lysosomes (Heckmann and Green, 2019; Heckmann et al., 2017; 2019; Martinez et al., 2011; 2015). LAP has been described mainly in professional phagocytes like macrophages, microglia, and dendritic cells that actively take up bacteria, opsonized particles, or dead cells. The process involves specific cargo receptors such as toll-like receptors, immunoglobulin receptors, and the phosphatidylserine receptor TIM4, respectively. While LAP activation by these receptors is poorly understood, it is independent of the ULK1–FIP200–ATG13–ATG101 complex. However, it shares the core components VPS34– VPS15–Beclin1 of the PI-3-kinase complex of canonical autophagy, but in combination with the LAP-specific partners UVRAG and Rubicon. Production of PI3P is required for LAP to recruit the NOX2 complex (NADPH oxidase 2, generating reactive oxygen species) and the ATG16L1 LC3 conjugation system, but not to recruit WIPI proteins, since they were shown to be dispensible (Heckmann and Green, 2019; Heckmann et al., 2017).

So far, little is known about selective autophagy of damaged early endosomes. Disrupting endosomes upon uptake of transfection reagent-coated latex beads showed a requirement for ubiquitination and for direct ATG16L1-binding to ubiquitin (Fujita et al., 2013). Alternatively, lysosomotropic agents like chloroquine and monensin have been employed which caused swelling of acidic compartments due to osmotic imbalance (Florey et al., 2015; Jacquin et al., 2017; Mauthe et al., 2018). They induce autophagy of the endolysosomal compartments from early and late endosomes to lysosomes, while simultaneously blocking autophagic flux by inhibiting fusion of autophagosomes with lysosomes (Mauthe et al., 2018). Surprisingly, chloroquine-induced LC3 lipidation was found to be independent of ATG13 (Florey et al., 2015; Jacquin et al., 2017). As a morphologically distinctive model of an endosomal compartment, entotic phagosomes or latex bead-containing phagosomes were analyzed upon treatment with chloroquine or monensin to induce LC3 recruitment. PI3P production was not induced on chloroquine-treated entotic vacuoles, nor did PI-3-kinase inhibition affect LC3 recruitment to these compartments, which showed a single-membrane morphology (Florey et al., 2015). p62 and NDP52 were not detected on chloroquine-treated entotic vacuoles, indicating that they were not ubiquitinated and thus most likely not ruptured. This was supported by the finding that swollen Lamp1-positive lysosomes due to chloroquine or monensin treatment were negative for galectin3 (Jacquin et al., 2017). These findings suggested that LC3 lipidation of these vacuoles was due to noncanonical autophagy, similar to LAP. Unlike starvation-induced autophagy, recruitment of LC3 to latex bead-containing phagosomes treated with monensin was independent of the FIP200-binding domain of ATG16L1, but dependent on its WD domain (Fletcher et al., 2018), indicating a further mechanistic difference of this system to starvation-induced autophagy. In contrast, however, Mauthe et al. (2018) found chloroquine treatment to induce lactate dehydrogenase sequestration, characteristic of canonical autophagy via phagophores, in a manner sensitive to PI-3 kinase inhibition, pointing to the production of PI3P.

Endosomes are dynamic organelles that receive endocytic cargo from the plasma membrane and exocytic material from the trans-Golgi for sorting to late endosomes and lysosomes, to the cell surface via recycling endosomes, or back to the Golgi (Naslavsky and Caplan, 2018). Endosomal identity is defined by specific Rab GTPases, their effectors, and by characteristic phosphoinositides. At early endosomes, Rab5 is the hallmark GTPase that activates VPS34/p150 to produce PI3P and recruits early endosome antigen 1 (EEA1) and Rabenosyn-5, two multivalent proteins that also bind to PI3P and act as membrane tethers to mediate homotypic endosome fusion. Rab5·GTP and PI3P are also responsible for recruitment of the ESCRT complexes (endosomal sorting complexes required for transport) to form intraluminal vesicles and of the Mon1/Ccz1 complex to activate Rab7 and deactivate Rab5 in the process of Rab conversion during maturation from early to late endosomes (Huotari and Helenius, 2011; Poteryaev et al., 2010).

Rab5 activity is regulated by a complex of Rabaptin5 and Rabex5, the GEF of Rab5. Rabaptin5 contains two binding domains for Rab4·GTP, at least one of which is required for recruitment to the membrane, and two further binding sites for Rab5·GTP, which are not (Kälin et al., 2016). Rabex5 and specifically its N-terminal ubiquitin-binding domain (Mattera and Bonifacino, 2008; Mattera et al., 2006) are also necessary for membrane

bioRxiv preprint doi: https://doi.org/10.1101/2020.09.01.277764; this version posted September 1, 2020. The copyright holder for this preprint (which was not certified by peer review) is the author/funder. All rights reserved. No reuse allowed without permission.

recruitment. This suggests that the Rabaptin5–Rabex5 complex is recruited mainly by Rab4 and (mono-)ubiquitinated cargo to activate Rab5 in a feed-forward manner (Kälin et al., 2016; 2015).

To identify potential yet unknown interactors of Rabaptin5, we performed a yeast two-hybrid screen and discovered FIP200 as a novel binding partner. We found that Rabaptin5 selectively targets autophagy to early endosomes damaged upon chloroquine or monensin treatment by interacting with FIP200 and with the WD domain of ATG16L1. Our results indicate a Rabaptin5-dependent mechanism for canonical selective autophagy of broken early endosomes. In addition, we show that Rabaptin5 initiates autophagy of early *Salmonella*-containing vacuoles and is thus responsible for killing a significant fraction of bacteria early upon infection.

RESULTS

FIP200 is a novel interactor of Rabaptin5 on early endosomes

To identify new interaction partners of Rabaptin5, we used human Rabaptin5 as a bait for a yeast two-hybrid screen with a HeLa cell prey library. The screen reproduced the known interactions of Rabaptin5 with itself and with Rabex5, but also revealed new candidates (Suppl. Table S1). Very interestingly, the screen detected FIP200 (Figure 1A and B), a component of the ULK1/ATG13 autophagy initiator complex, as a high confidence interactor of Rabaptin5. The smallest isolated interacting fragment encompassed residues 281–439 of FIP200, a segment outside the coiled-coil regions of the protein (Figure 1C). Importantly, an interaction of FIP200 with Rabaptin5 could be confirmed in HeLa and HEK293A cells by co-immunoprecipitation from cell lysates (Figure 1D).

By yeast two-hybrid testing of different protein fragments, the interacting segment in Rabaptin5 was identified to be the coiled-coil domain CC2-1 (Figure 1A and B), where also Rabex5 and the GAT domain of GGA proteins have been shown to bind (Zhang et al., 2014; Zhu et al., 2004). Since this domain and binding of Rabex5 are important for Rabaptin5 recruitment to early endosomes (Kälin et al., 2015), specific disruption of FIP200-binding by its deletion is not possible. Deletion of the segment 280–440 of FIP200 that is sufficient for interaction with Rabaptin5 in the two-hybrid assay was found to be necessary for co-immunoprecipitation of Rabaptin5 (Figure 1E). Unfortunately, deletion of this segment also strongly reduced co-immunoprecipitation of ATG13 and to a lesser extent of ULK1 with FIP200 (Figure 1F and G, resp.), indicating that it did not specifically abrogate binding to Rabaptin5, but also destabilized the incorporation of FIP200 into the ULK1 initiator complex. This is in line with recent structural data indicating that overlapping residues 435–442 are important for protein stability and that residues 443-450 of FIP200, right next to the Rabaptin5-binding region, binds ATG13 (Shi et al., 2020). The FIP200Δ280–440 mutant thus cannot help to define the role of Rabaptin5 in autophagy.

FIP200 transfected alone in HeLa cells localized to small intracellular puncta throughout the cell (Suppl. Figure S1A), corresponding to steady-state autophagosomes (Hara et al., 2008). When expressed together with wild-type Rabaptin5, they colocalized in slightly larger structures (Suppl. Figure S1B). Similarly, FIP200 colocalized with the cotransfected early endosomal markers Rab4 and Rab5, but not with the late endosomal marker Rab7 (Suppl. Figure S1C–D). This observation supports a function of FIP200 on early Rabaptin5-positive endosomes.

Chloroquine treatment induces autophagy of Rabaptin5-positive early endosomes

To assess a potential involvement of Rabaptin5 in autophagy at early endosomes, we employed chloroquine treatment as in previous studies (e.g. Mauthe et al., 2018). To be able to easily detect Rabaptin5-positive early endosomes by immunofluorescence without transient transfection, we generated a stable HEK293A cell line moderately overexpressing Rabaptin5 approximately 5 times (HEK^{+Rbpt5}; Figure 2A). Incubation of these cells with 60 μM chloroquine for 30 min indeed produced swollen structures appearing as small rings positive for

bioRxiv preprint doi: https://doi.org/10.1101/2020.09.01.277764; this version posted September 1, 2020. The copyright holder for this preprint (which was not certified by peer review) is the author/funder. All rights reserved. No reuse allowed without permission.

Rabaptin5 and transferrin receptor and thus identifiable as early endosomes (Figure 2B). In transfected cells expressing moderate levels of mCherry-galectin3, this lectin was found to be recruited to the Rabaptin5-positive endosomes (Figure 2C), indicating membrane rupture. They also stained positive for ubiquitin (Figure 2D), consistent with exposure of lumenal protein domains to the cytosol. These rings further stained for the early autophagy components WIPI2 and ATG16L1, but not for the late component LC3B (Figure 2E–G). Colocalization of WIPI2 and ATG16L1 and the absence of colocalization of LC3B was not only observed qualitatively on large Rabaptin5-positive rings, but also globally as quantified using Manders' colocalization coefficients (Figure 2H–J): the fraction of Rabaptin5 on WIPI2- or ATG16L1-positive structures (M1) and the fractions of these two proteins on Rabaptin5-positive structures (M2) were significantly increased already after 15 min chloroquine treatment and similarly after 30 min. No significant effect was observed for LC3B, suggesting that late autophagosomes that accumulate due to the block in autophagic flux have lost Rabaptin5.

Chloroquine-induced autophagy depends on Rabaptin5, FIP200, ATG13, and ATG16L1, but not ULK1

Upon longer exposure of 150 min to chloroquine or to Torin1, an inhibitor of mTOR mimicking starvation-induced autophagy, control cells showed a strong increase in the numbers of both early WIPI2-positive and late LC3B-positive autophagosomal puncta (Figure 3). Silencing of FIP200 expression by RNA interference blocked this increase of WIPI2 autophagosomes completely and of LC3B autophagosomes to a large extent for both treatments. Silencing of Rabaptin5 produced the same strong inhibitory effect specifically on chloroquine-induced WIPI2 structures and a smaller reduction of LC3B structures, but did not affect autophagy induction by Torin1. This result indicates that Rabaptin5 is specifically required to initiate FIP200-dependent autophagy of damaged endosomes and is not involved in starvation-induced autophagy regulated by mTOR. The observation that knockdown of Rabaptin5 as well as of FIP200 appears less effective in reducing LC3B structures with chloroquine is likely due to stabilization of late phagophagosomes by inhibition of autophagic flux (e.g. Mauthe et al., 2018).

In the same manner, we tested for an involvement of ULK1 and ATG13, the two main partners of FIP200 in the classical pre-initiation complex (Figure 4A and B). Silencing of ULK1, which inhibited starvation- and Torin1-induced autophagy (Suppl. Figure S2), did not significantly reduce chloroquine induction of WIPI2- nor LC3B-positive autophagosomes. In contrast, ATG13 silencing essentially blocked an increase of WIPI2 puncta and strongly reduced LC3B structures (Figure 4A and B), just like silencing of FIP200 or Rabaptin5 did. Silencing of ATG16L1, which recruits the ATG5/12 E3-like enzyme complex for LC3 lipidation, also blocked formation of WIPI2 puncta and significantly reduced LC3B autophagosomes induced by chloroquine (Figure 4C and D). ATG16L1 thus appears to be required to recruit or stabilize WIPI2. Our data suggest that in our system chloroquine treatment induces endosomal autophagy via the FIP200–ATG13 complex, but not involving ULK1.

Chloroquine induced autophagy depends on galectin3 and p62

The observation that chloroquine-induced Rabaptin5-positive swollen endosomes recruited galectin3 and were positive for ubiquitin (Figure 2C and D) indicated membrane rupture. We therefore tested the requirement for galectin3 and p62 as a candidate SAR (Figure 5). siRNA-mediated silencing of both proteins clearly reduced chloroquine-induced WIPI2-positive autophagosomes, while – as expected – Torin1-induced autophagy was not affected. This confirms membrane disruption by chloroquine and indicates an involvement of galectin3 and p62 in this type of selective autophagy. LC3B structures were not significantly reduced, perhaps because other galectins and SARs may contribute as well. Since chloroquine inhibits autophagic flux, accumulating LC3B-positive structures are likely less sensitive to partial inhibition. Organelle rupture argues against a general LAP-like process, but supports canonical selective autophagy.

Rabaptin5 binds to the WD domain of ATG16L1 via a conserved interaction motif

Previously, autophagy of galectin3-positive lysosomes specifically induced by Leu-Leu-O-Me (LLOMe), which is condensed into a membranolytic polymer by cathepsin C, was found to depend on TRIM16 (Chauhan et al.,

bioRxiv preprint doi: https://doi.org/10.1101/2020.09.01.277764; this version posted September 1, 2020. The copyright holder for this preprint (which was not certified by peer review) is the author/funder. All rights reserved. No reuse allowed without permission.

2016). TRIM16 was shown to bind both galectin3 and the coiled-coil domain of ATG16L1. In search for partners of Rabaptin5 on the surface of chloroquine-damaged endosomes, we performed co-immunoprecipation experiments. Upon immunoprecipitation of Rabaptin5, galectin3 could be co-immunoprecipitated, both without treatment and with increasing efficiency after chloroquine treatment of the cells (Suppl. Figure S3A). In contrast, no co-immunoprecipitation could be detected of Rabaptin5 and TRIM16 (Suppl. Figure S3B).

To test whether Rabaptin5 might connect galectin3 with ATG16L1 on endosomes just like TRIM16 does on lysosomes, we looked for an interaction between Rabaptin5 and ATG16L1. Indeed, ATG16L1 was co-immunoprecipitated with Rabaptin5 already from untreated cells, but even more extensively after 30 min of chloroquine treatment (Figure 6A). Interestingly, the interaction appeared to decrease after 2 h of chloroquine treatment. This time-dependence is consistent with a dynamic interactome starting with Rabaptin5 connecting to the FIP200 and ATG16L1 complexes and then evolving to release Rabaptin5 before maximal LC3 recruitment is achieved (Figure 2G and J).

Co-immunoprecipitation of ATG16L1 with Rabaptin5 was lost upon deletion of the WD-repeat domain in ATG16L1 (Figure 6B). Rabaptin5 thus interacts differently with ATG16L1 than TRIM16, which was shown to bind to the coiled-coil domain (Chauhan et al., 2016). In contrast, the membrane protein TMEM59, a promoter of selective autophagy of *Staphylococcus aureus*-containing phagosomes, had previously been shown to bind to the WD domain (Boada-Romero et al., 2013). A 19-amino acid peptide motif containing four essential residues had been identified to mediate this interaction. Similar largely conserved motifs were also found in NOD2, a protein known to recruit ATG16L1 at bacterial entry sites, and in TLR2 that promotes LC3 lipidation at phagosomes. Interestingly, Rabaptin5 also contains a sequence (residues 507–518) that complies with this consensus motif (Figure 6C). Mutation of the three most important residues of this motif to alanines (Y507A/W515A/L518A in Rabaptin5AAA), which in TMEM59 completely inactivated ATG16L1 binding, also eliminated co-immunoprecipitation of ATG16L1 with mutant Rabaptin5 (Figure 6D).

Binding of Rabaptin5 to ATG16L1 is essential for endosomal autophagy

To demonstrate the importance of this interaction between Rabaptin5 and ATG16L1, we produced a Rabaptin5 knockout HEK293A cell line (Rbpt5-KO) by CRISPR/Cas9 gene inactivation. By transfecting wild-type Rabaptin5 or the triple mutant Rabaptin5-AAA, we produced the stable cell lines Rbpt5-KO+wt and Rbpt5-KO+AAA that produced similar Rabaptin5 levels as the original HEK293A cell line (Figure 7A). As a control, we also generated a CRISPR/Cas9 knockout cell line for FIP200. Again, we analyzed WIPI2- and LC3-positive autophagosomes before and after chloroquine treatment for 150 min (Figure 7B and C, and Suppl. Figure S4). While overexpression of Rabaptin5 resulted in a slight increase of steady-state and chloroquine-induced WIPI2 puncta, Rabaptin5 knockout left the steady-state levels unchanged and eliminated chloroquine-induced formation of WIPI2 autophagosomes (Figure 7B). Re-expression of wild-type Rabaptin5 rescued autophagosome induction by chloroquine, while Rabaptin5-AAA did not. This result suggests that the interaction of Rabaptin5 with ATG16L1 is essential for early endosomal autophagy upon chloroquine damage.

Rabaptin5 knockout also reduced the chloroquine-dependent increase of LC3B-positive puncta (Figure 7C), consistent with inhibition of initiation of endosomal autophagy, while LC3 autophagosomes accumulate due to the block of autophagic flux. Again, re-expression of wild-type Rabaptin5, but not Rabaptin5-AAA, rescued formation of LC3B-positive structures. FIP200 knockout strongly reduced both steady-state and chloroquine-induced autophagosomes positive for either WIPI2 or LC3B, consistent with an essential role for both steady-state and endosomal autophagy.

These results with stable cell lines confirm those with siRNA knockdown of Rabaptin5 or FIP200 of Figure 3. It should be noted that the numbers of WIPI2 and LC3B puncta were consistently higher under knockdown conditions even at steady-state. A direct comparison of untreated and control siRNA transfected cells showed this to be nonspecifically caused by siRNA transfection, reflected in higher numbers of autophagosomes and an increased ratio of lipidated / unlipidated LC3B (Suppl. Figure 5).

bioRxiv preprint doi: https://doi.org/10.1101/2020.09.01.277764; this version posted September 1, 2020. The copyright holder for this preprint (which was not certified by peer review) is the author/funder. All rights reserved. No reuse allowed without permission.

Immunoblot analysis of LC3B lipidation upon chloroquine treatment (Figure 7D and E) showed the expected increase of LC3B-II in wild-type and Rabaptin5-overexpressing cells, which was reduced in Rabaptin5 knockout cells and rescued by re-expression of wild-type Rabaptin5, but not of the AAA mutant.

We furthermore quantified colocalization of Rabaptin5 and ATG16L1 or WIPI2 upon chloroquine treatment for 0, 15, or 30 min in Rabaptin5-overexpressing cells and in knockout cells re-expressing wild-type or AAA mutant Rabaptin5 (Figure 7F and G). Colocalization with either autophagy protein was lower and hardly induced in knockout cells expressing the Rabaptin5-AAA mutant unable to bind ATG16L1, demonstrating that this interaction is required to induce endosomal autophagy.

There are a number of interconnections between autophagy and endosomes (Birgisdottir and Johansen, 2020). One should thus consider the possibility that absence or mutation of Rabaptin5 might alter endosome properties in a way that indirectly affects chloroquine-induced autophagy. We therefore confirmed that chloroquine induces early endosome swelling also in Rabaptin5-KO cells by immunofluorescence microscopy of EEA1 (Suppl. Figure 6A). Rabaptin5 deletion did not affect autophagic flux, since expression of tandem fluorescent tagged RFP-GFP-LC3 containing an acid-sensitive GFP and a pH-insensitive RFP (Kimura et al., 2007) showed an indistinguishable fraction of autophagosomes (red/green double-positive LC3 puncta) and autolysosomes (red-only LC3 puncta) in HEK293A and Rabaptin5-KO cells, without treatment or upon induction of autophagy by starvation or Torin1 treatment (Suppl. Figure 6B and C).

To further exclude the possibility that the triple AAA mutation inactivated the function of Rabaptin5 in endosomal maturation and thus perhaps affected endosomal autophagy indirectly, we analyzed the number of lysosomal structures in the different HEK cell lines by lysotracker staining (Figure 6H). The marked reduction of lysosomes upon Rabaptin5 knockout was completely rescued by re-expression of wild-type Rabaptin5 and also by Rabaptin5-AAA, demonstrating that the endosomal function of the mutant protein was intact (Figure 6I).

Monensin-induced endosomal autophagy also depends on Rabaptin5 and its interaction with ATG16L1

Chloroquine is protonated and trapped within acidified endosomes and lysosomes, osmotically promoting compartment swelling by water influx. Monensin promotes the exchange of protons for osmotically active monovalent cations like Na^+ and thus results in osmotic swelling of acidified compartments in a different way. Monensin treatment of HEK^{+Rbpt5} cells rapidly produced swollen Rabaptin5-positive early endosomes that stained positive for ATG16L1 and WIPI2 (Suppl. Figure S7A), just like chloroquine treatment (Figure 2E and F). Similarly, overall colocalization of ATG16L1 and WIPI2 with Rabaptin5-positive structures increased in Rabaptin5 overexpressing HEK^{+Rbpt5} cells and in Rabaptin5-knockout cells re-expressing wild-type Rabaptin5, but not in knockout cells expressing the Rabaptin5-AAA mutant that is unable to bind to ATG16L1 (Suppl. Figure S7B and C). The increase in total WIPI2-positive structures upon monensin treatment was also dependent on Rabaptin5, since it was abolished upon knockout of Rabaptin5 and recovered upon re-expression of wild-type Rabaptin5, but not by the AAA mutant (Suppl. Figure S7D). The effect on the induction of LC3B-positive structures was less clearly dependent on Rabaptin5 (Suppl. Figure S7E), likely because of the inhibitory effect of monensin on autophagic flux.

Rabaptin5 targets *Salmonella*-containing vacuoles to autophagy

As *Salmonella enterica* enters the host cell, its surrounding phagosomal membrane quickly acquires the characteristics of early endosomes through fusion with Rab5-positive endosomes (LaRock et al., 2015; Levin et al., 2016; Steele-Mortimer et al., 1999). The *Salmonella*-containing vacuole (SCV) is thus positive for Rab5, Rabaptin5/Rabex5, EEA1, transferrin receptor (TfR), and the PI-3 kinase VPS34. Perforation of the early SCV membrane by the Type III secretion system 1 (T3SS-1) results in binding of cytosolic galectins and ubiquitination to activate antibacterial autophagy to the SCV membrane (LaRock et al., 2015). Because of this similarity of the early SCV with damaged early endosomes, we tested the role of Rabaptin5 in autophagy of *Salmonella* early after infection.

bioRxiv preprint doi: https://doi.org/10.1101/2020.09.01.277764; this version posted September 1, 2020. The copyright holder for this preprint (which was not certified by peer review) is the author/funder. All rights reserved. No reuse allowed without permission.

We first infected HeLa cells with *Salmonella enterica* serovar Typhimurium with or without siRNA-mediated silencing of Rabaptin5 or FIP200 and determined the number of phagocytosed live bacteria after 0, 1, 3 and 6 h (Figure 8A). For this, bacteria were gently centrifuged onto the cell layer for 5 min at 37°C and further incubated for 10 min. Bacteria that had not entered the cells were thoroughly washed away. For further incubation, the medium was supplemented with gentamycin to eliminate any remaining extracellular bacteria. Yet, even immediately after infection, confocal immunofluorescence microscopy confirmed that essentially all cell-associated bacteria were internalized. The infection efficiency was not affected by silencing Rabaptin5 or FIP200 (~14% of cells infected; Suppl. Figure S8). At different time points, cells were lysed and plated out to determine the number of live bacteria.

Within the first hour of infection, ~80% of initially internalized bacteria were killed, after which live cell numbers increased again. Part of the observed initial killing is due to autophagy, since knockdown of FIP200 almost doubled the number of live cells 1 h after infection (Figure 8A, right). Silencing of Rabaptin5 expression was at least as effective, indicating a contribution of Rabaptin5 to early bacterial killing. These findings were confirmed by experiments using our stable HEK293A cell lines (Figure 8B). Only 25% of internalized *Salmonella* survived the first hour in parental HEK293A cells, whereas overexpression of Rabaptin5 in HEK^{+Rbpt5} cells reduced this fraction by half and knockout of Rabaptin5 doubled it. Re-expression of the wild-type protein in knockout cells recovered wild-type levels of survival, while expression of the mutant Rabaptin5-AAA that is unable to bind ATG16L1 did not.

These results suggest that Rabaptin5 recruits autophagy to the damaged membrane of SCVs and contributes to killing of phagocytosed *Salmonella*. To confirm this concept, bacteria infecting the different HEK293A cell lines were analyzed by immunofluorescence microscopy for colocalization with TfR as a marker for early endosomal membrane identity and for LC3B as an autophagy marker (Figure 8C). Right after infection, while virtually all bacteria were intracellular, more than half of them were negative for both markers. This fraction rapidly declined for the next 15 min and the fraction in a TfR-positive environment with or without LC3B increased significantly, consistent with increasing acquisition of endosomal markers of the SCVs by fusion with early endosomes.

In wild-type HEK293A cells and Rabaptin5-overexpressing HEK^{+Rbpt5} cells, the predominant population 5–30 min after infection was that of *Salmonella* in double positive (TfR+/LC3B+) SCV–autophagosomes (Figure 8C). In Rabaptin5 knockout cells, this population was reduced in favor of a majority of TfR single-positive SCVs as a result of reduced autophagy initiation. Expression of Rabaptin5-AAA did not change this situation, confirming that the interaction with ATG16L1 is required to initiate autophagy of SCVs. At the same time, it shows that the phenotype of the knockout cells is not just the result of reduced endosome maturation in the absence of Rabaptin5, since the AAA mutant is functional for its other endosomal functions. In FIP200 knockout cells TfR+/LC3B+ SCVs were also reduced, as expected.

In summary, Rabaptin5, in addition to its function as a regulator of early endosome identity and endosomal maturation, plays an unexpected role in initiating autophagy of damaged early endosomes and bacteria-containing phagosomes via interaction with FIP200 and ATG16L1.

DISCUSSION

So far, Rabaptin5 had been characterized as a regulator of Rab5 activity by complex formation with Rabex5, the GDP/GTP exchange factor of Rab5. In addition it had been shown to bind to Rab4·GTP and Rab5·GTP, the hallmark Rab proteins of early endosomes (Horiuchi et al., 1997; Kälin et al., 2015; 2016; Lippé et al., 2001; Mattera et al., 2006). Rabaptin5 thus was known to contribute to endosome identity and maturation (Huotari and Helenius, 2011). Consistent with these functions, we found here that the number of lysosomes, the endpoint

bioRxiv preprint doi: https://doi.org/10.1101/2020.09.01.277764; this version posted September 1, 2020. The copyright holder for this preprint (which was not certified by peer review) is the author/funder. All rights reserved. No reuse allowed without permission.

organelles of the endosomal pathway, was increased by overexpression and reduced upon knockout of Rabaptin5 (Figure 7H and I).

In this study, we identified FIP200 and ATG16L1 as novel interactors of Rabaptin5 and thus an additional unexpected role in autophagy. Endosomes – specifically recycling endosomes – were previously implicated as a source of membranes and of ATG9 and ATG16L1 for growing phagophores (Knævelsrud et al., 2013; Popovic and Dikic, 2014; Puri et al., 2013). Rab11A-positive recycling endosomes were found to act as a platform for autophagosome assembly mediated by the interaction of WIPI2 with PI3P and Rab11A (Puri et al., 2018). These recycling endosomes were demonstrated to be distinct from Rab5- and thus also Rabaptin5-positive early (sorting) endosomes. While Rab11A was shown to be broadly important for starvation-induced autophagy as well as mitophagy (Puri et al., 2018), silencing of Rabaptin5 did not affect Torin1-induced autophagy, but specifically autophagy induced by chloroquine or monensin and of SCVs.

We found chloroquine-induced Rabaptin5-positive swollen endosomes to be broken, since they recruited galectin3 and were stained positive for ubiquitin, besides WIPI2 and ATG16L1 (Figure 2). Chloroquine-induced WIPI2 autophagosomes were strongly reduced by depletion of galectin3 and p62, indicating that exposure of lumenal proteins triggered autophagy (Figure 5). They were also reduced by silencing of Rabaptin5 and of FIP200 and ATG13, but not ULK1 (Figures 3 and 4). LC3B autophagosomes/autolysosomes were similarly affected, but to a lesser extent, most likely because chloroquine, by inhibiting autophagic flux, increases their life-time.

The involvment of galectin3 and p62, and of the FIP200 initiator complex is in full agreement with canonical selective autophagy (e.g. Turco et al., 2019; Vargas et al., 2019) upon chloroquine treatment and supported by LDH sequestration by chloroquine-induced phagophores (Mauthe et al., 2018). In these respects, it is similar to lysophagy induced by LLOMe treatment (Chauhan et al., 2016; Kumar et al., 2017; Maejima et al., 2013). However, it contradicts a noncanonical LAP-like mechanism that was proposed using entotic vacuoles or latex bead-containing phagosomes as model organelles to study the effects of chloroquine or monensin treatment. Here, LC3 was recruited directly to the single membrane vacuole without PI3P production or WIPI involvment, and without recruitment of p62 or NDP52 (Fletcher et al., 2018; Florey et al., 2015). LC3 recruitment was found to be independent of ATG13 and of the FIP200-binding domain of ATG16L1, arguing against an involvment of the ULK1/FIP200 complex (Fletcher et al., 2018; Florey et al., 2015; Jacquin et al., 2017). Clearly, chloroquine and monensin trigger very different responses on large entotic vacuoles or phagosomes than on regular early endosomes.

Interestingly, silencing of ATG16L1 did not only affect downstream LC3B puncta, but also reduced WIPI2 structures. This was surprising, since depletion of WIPI1 or WIPI2 was previously shown to strongly reduce recruitment of ATG16L1, suggesting WIPI1/2 to be upstream of ATG16L1 (Bakula et al., 2017; Dooley et al., 2014; Dudley et al., 2019). Our result suggests a positive feedback of ATG16L1 recruitment on WIPI2 stability on membranes, similar to the finding that PI3P stabilizes the upstream ULK complex on phagophores by directly interacting with ATG13 (Karanasios et al., 2013). Recently, it was also shown that the PI 3-kinase complex and WIPI2 mutually promote the recruitment of each other in a positive feedback loop (Fracchiolla et al., 2020). The many interactions between the components of the autophagy machinery reveal a complex network that goes beyond a linear chain of events in the development of autophagosomes (Dudley et al., 2020), but provides a degree of robustness and redundancy and may adapt to different cargos and targeting mechanisms.

Most importantly, we found Rabaptin5 to be essential to recruit the autophagy machinery to damaged endosomes by direct binding to FIP200 and ATG16L1. In this way, Rabaptin5 connects the protein network of early endosomes with the developing interactome of autophagy (illustrated schematically in Suppl. Figure S9). The observation that significant colocalization of Rabaptin5 and LC3B could not be observed, suggests a dynamic remodeling of the network in which Rabaptin5 is lost before LC3B recruitment peaks. It is not known whether and how Rabaptin5 is regulated to switch on its autophagy-activating function upon membrane rupture, except that it associates (directly or indirectly) with galectin3. With its affinity for FIP200 and ATG16L1, Rabaptin5 may facilitate formation of an active autophagy interactome, when membrane rupture, galectin

bioRxiv preprint doi: https://doi.org/10.1101/2020.09.01.277764; this version posted September 1, 2020. The copyright holder for this preprint (which was not certified by peer review) is the author/funder. All rights reserved. No reuse allowed without permission.

binding, ubiquitination, and p62 accumulation produce additional binding interactions beyond a certain activation threshold. Consistent with this mechanism, FIP200 and ATG16L1 could be co-immunoprecipitated with Rabaptin5 even at steady-state, but to a higher degree upon treatment with chloroquine.

Rabaptin5 binds to the WD domain of ATG16L1 via an interaction motif ^{507}**Y**RLVS**E**TE**W**NL**L**^{518} based on a conserved consensus initially identified in TMEM59, NOD2, and TLR2 to promote autophagy, particularly in the context of bacterial phagosomes (Boada-Romero et al., 2013). Rabaptin5 with three of the key residues in this sequence mutated to alanines could not rescue chloroquine-induced WIPI2 and LC3B puncta beyond the level of the Rabaptin5 knockout and did not induce colocalization with WIPI2 or ATG16L1. This suggests that, in the context of a damaged early endosomes, Rabaptin5 makes an essential contribution to recruit ATG16L1. The contribution of the interaction with FIP200 could not be assessed, since deletion of the interacting segment in Rabaptin5 (residues 547–666; CC2-1) abolishes Rabex5-binding and membrane recruitment (Kälin et al., 2015) and in FIP200 destabilized complex formation with ATG13 and ULK1.

For *Salmonella*-containing vacuoles, canonical autophagy is well established (LaRock et al., 2015). *Salmonella* manipulates its host by secreting effectors via two Type III secretion systems (T3SS) into the host cytosol. T3SS-1 is required for internalization into SCVs. As SCVs are further acidified, T3SS-2 is induced and its effectors mediate maturation to *Salmonella*-induced filaments, where bacteria proliferate. However, T3SS-1 also damages the SCV membrane. Bacteria that are completely released into the cytosol hyperproliferate while being direct targets of ubiquitination and autophagy. In contrast, damaged SCVs are recognized by selective autophagy in a similar manner as damaged endosomes: exposure of lumenal protein domains and glycans trigger the binding of galectin3 and 8 (Fujita et al., 2013; Thurston et al., 2012) and poly-ubiquitination; SARs including p62 and NDP52 are recruited (Thurston et al., 2012; Zheng et al., 2009) and SCVs are surrounded by phagophores (Fujita et al., 2013; e.g. Kageyama et al., 2011; Kishi-Itakura et al., 2020).

Because of the similarities between autophagy of SCVs and of damaged endosomes, we tested a potential role of Rabaptin5 in the early phase of *Salmonella* infection. We found that autophagic elimination of *Salmonella* during the first hour post infection, when the SCVs most resemble early endosomes, strongly depended on Rabaptin5 and its ability to bind ATG16L1. In wild-type HeLa and HEK293A cells, 70–80% of internalized bacteria were killed within the first hour (Figure 8A and B). Knockdown or knockout of Rabaptin5 reduced this number to approximately 50%, i.e. to the same extent as silencing of FIP200 did. The same effect was observed, when wild-type Rabaptin5 was replaced by a mutant Rabaptin5 with a triple mutation eliminating its interaction with ATG16L1. Residual killing may be due to autophagy of free bacteria or of later stages of SCV maturation which have lost Rabaptin5 and Rab5 already.

Our study thus shows that Rabaptin5 has dual functions: in addition to its role as a regulator of early endosome identity and endosome maturation, it contributes to initiate and promote autophagy, when endosomes are damaged by chemical agents or by pathogens.

bioRxiv preprint doi: https://doi.org/10.1101/2020.09.01.277764; this version posted September 1, 2020. The copyright holder for this preprint (which was not certified by peer review) is the author/funder. All rights reserved. No reuse allowed without permission.

MATERIALS AND METHODS

Antibodies and reagents

Mouse anti Transferrin Receptor (OKT8 mouse monoclonal hybridoma, kind gift of Dr. H. Farhan, 1:1000), mouse anti-Rbpt5 (610676, BD Transduction Laboratories, 1:1000) and rabbit anti-Rabaptin5 antibodies (NBP1-47285, Novus Biologicals, 1:500) were used for immunofluorescence and Western blotting, rabbit anti-FIP200 (12436S, Cell Signaling, 1:1000) was used for Western blot and co-immunoprecipitation. Mouse anti-tubulin (kind gift of Dr. H. Farhan, 1:1000) was used for immunoblotting. Rabbit anti-Galectin3 (1:1000; Abcam ab31707), rabbit anti-ATG16L1 (8089, Cell Signaling, 1:1000), rabbit anti-MYC (GTX29106, GeneTEX, 1:5000) rabbit anti-mCherry (PA5-34974, Invitrogen, 1:1000) and rabbit EEA1were (1:1000; Abcam Ab2900 used for co-immunoprecipitations. Mouse anti-WIPI2 (ab105459, Abcam, 1:500) and rabbit anti LC3B (3868S, Cell Signaling, 1:1000 WB, 1:400 IF) were used for western blot and immunofluorescence. Rabbit anti-TRIM16 (NB100-59772, Novus Biologicals, 1:1000), rabbit anti-ULK1 (#8054S, Cell Signaling, 1:1000) and rabbit anti ATG13 (#13468S, Cell Signaling, 1:1000) were used for immunoblotting. Mouse anti-Ubiquitin was used for immunofluorescence (SC-8017, Santa Cruz, 1:500). Alexa-Fluor-488- or Alexa-Fluor-568-tagged donkey anti-mouse- or anti-rabbit-immunoglobulin antibodies (A32766, A32790, A10042, A10037, Molecular Probes, 1:200) and Alexa-Fluor-633 goat anti mouse (A-21050, Molecular Probes, 1:200) were used as secondary antibodies for immunofluorescence, and horseradish-peroxidase-coupled goat anti-mouse- or anti-rabbit-immunoglobulin antibodies (A0168, A0545, Sigma Immunochemicals, 1:5000) in combination with the enhanced chemiluminescence reaction kit (Amersham Pharmacia Biotech)

Plasmids and mutagenesis

Plasmids of human Rabaptin5, RFP-Rab5 (pSI-AAR6_Rab5), and GFP-Rab7 (pSI-AAL6_Rab7) were described in Kälin et al. (2015). The cDNA of human FIP200 was purchased from OriGene (SC114884), pmCherry_Gal3 was a gift from Hemmo Meyer (Addgene plasmid #85662) (Papadopoulos et al., 2017), pSpCas9(BB)-2A-GFP (PX458) was a gift from Feng Zhang (Addgene plasmid #48138) (Ran et al., 2013), and mCherry-ATG16L1 was a kind gift from Sharon Tooze, London. Mutations were introduced by PCR mutagenesis.

Cell culture and transfection

HeLaα and HEK293A cells were grown in Dulbecco's modified Eagle's medium (DMEM) supplemented with 10% fetal calf serum (FCS), 100 units/ml penicillin, 100 units/ml streptomycin, and 2 mM L-glutamine at 37°C at 7.5% CO_2.

To generate Rabaptin5- and FIP200-knockout cell lines in HEK293A cells, the gRNA sequences AGAGTGTGTACCTACAGTGC (Rabaptin5) and TGGGCGCCTCACCGTCAGGC (FIP200) extended with Bpi I overhangs were cloned into pSpCas9(BB)-2A-GFP, digested with Bpi I (Thermo Scientific, FD1014). 24 h after transfection, the plasmid containing cells were selected by fluorescence-activated cell sorting based on GFP expression. After 10 days of culture, single cells were sorted again for loss of GFP expression and expanded. Gene inactivation was confirmed by immunoblotting.

Transient transfections were performed using Fugene (Promega) or JetPRIME (Polyplus) and cells analyzed after 2 days. For stable expression, cells were transfected with the respective pcDNA3 constructs and subsequently selected with 2 mg/ml G418 (Geneticin from Thermo Fisher Scientific; 3 mg/ml for 10 days). Surviving cells were expanded in culture medium containing G418.

For knockdown experiments, siRNAs were purchased from Dharmacon Thermo Fisher Scientific (nontargeting siControl, D-001810-10-05; Rabaptin5 siRABEP1, L-017645-01; FIP200 siRB1CC1, M-021117-01-0005; siATG16L1, J-021033-11-0010; siATG13, L-020765-01; siULK1, L-005049-00). Cells were transfected with 20 nM siRNA and HiPerFect (QIAGEN), and used after 3 days.

bioRxiv preprint doi: https://doi.org/10.1101/2020.09.01.277764; this version posted September 1, 2020. The copyright holder for this preprint (which was not certified by peer review) is the author/funder. All rights reserved. No reuse allowed without permission.

Immunofluorescence microscopy and quantitation

Cells on coverslips were fixed with 3% paraformaldehyde (PFA) for 10 min at room temperature, quenched for 5 min with 50 mM NH_4Cl, washed with PBS, permeabilized with 0.1% Triton X-100 for 10 min, blocked with 3% BSA in PBS for 15 min, incubated for 1 h with primary antibodies in PBS with BSA, washed, and stained for 30 min with fluorescently tagged secondary antibodies in PBS with BSA. Coverslips were mounted in Fluoromount-G (Southern Biotech).

For LC3B and WIPI2 staining, fixation was performed with methanol or, when co-staining for Rabaptin5, with PFA/methanol. In the first case, cells were fixed for 15 min in –20°C methanol, permeabilized for 10 min with 0.3% Triton X-100, blocked for 30 min with 3% BSA in PBS, and incubated overnight with the primary antibody at 4°C. In the second case, cells were first fixed in 3% PFA for 1 min and then for 15 min in 100% –20°C methanol, permeabilized for 10 min with 0.1% Triton X-100, blocked for 15 min with 3% BSA in PBS, and incubated overnight with the primary antibody at 4°C. Secondary antibody was incubated in 3% BSA for 30 min at room temperature.

Images were acquired using an LSM700 confocal microscope or an API Delta Vision Core microscope with a 63x lens. All experiments were repeated at least three times. Images were analyzed with Fiji, using the JACoP plugin to determine Mander's colocalization coefficients. Quantitations were based on images of 11 fields typically containing 3–8 cells. To quantify colocalization between Rabaptin5 and mCherry-ATG16L1, transfected cells were fixed with PFA/methanol as above and stained for Rabaptin5. Images of at least 20 mCherry-ATG16L-expressing cells were analyzed per experiment.

To estimate the number of lysosomes, cells were loaded overnight with 450 nM Lysotracker Green (from Molecular Probes), fixed in 3% PFA, and imaged. Images for at least 15 cells per sample were quantified using Fiji.

To evaluate autophagic flux, HEK293A and Rabaptin5-KO cells were transduced with the Premo Autophagy Tandem Sensor RFP-GFP-LC3B Kit (Thermo Fisher Scientific) for 48 h and incubated with or without HBSS starvtion media or with 250 nM Torin1 for 3 h before fixation. GFP/RFP double-positive autophagosomes and GFP-negative/RFP-positive autolysosomes were quantified by fluorescence microscopy.

Co-immunoprecipitation

Cells were lysed with lysis buffer (0.5% Na-deoxycholate, 1% Triton X-100, 2 mM PMSF, protease inhibitor cocktail). Post-nuclear supernatants were incubated with antibody overnight at 4°C. Antigen–antibody complexes were collected with protein A-Sepharose for 2 h at 4°C, washed three times with lysis buffer, and subjected to immunoblot analyses.

Salmonella infection and immunofluorescence analysis

Wild-type *Salmonella enterica* serovar Typhimurium strain SL1344 was cultured in Luria broth (LB) overnight at 37°C with shaking, followed by dilution into 10 ml of fresh LB (1:33), and continued to grow under the same conditions for 3 h. One milliliter of bacteria was then centrifuged at 8,000×g for 2 min and resuspended in 1 ml of PBS. This suspension was diluted into DMEM + 10% FCS (no antibiotics) and added directly to HeLa or HEK293A cell lines to a multiplicity of infection of 100. The infected cell monolayers were centrifuged at 500×g for 5 min at 37°C to synchronize the infection and incubated 10 min at 37°C. The monolayers were then washed three times in PBS and then incubated in fresh culture medium with 100 µg/ml gentamycin. At 1 h post infection, the gentamycin concentration was reduced to 10 µg/ml. At designated time points, cells were washed three times with PBS and lysed in 500 µl of lysis buffer (PBS with 1% Triton X-100). Serial dilutions were plated onto LB agar plates (with 90 µg/ml streptomycin) to determine bacterial live cell count.

For microscopy, cells were infected with GFP-expressing *Salmonella* SL1344 as above, fixed after different times by the methanol fixation protocol, and incubated with anti-TfR and anti-LC3B antibodies in PBS with 3% BSA overnight at 4°C, followed by fluorescent secondary antibodies for 30 min at room temperature. Images were acquired using a Zeiss LSM700 confocal microscope and analysed in Fiji. To determine the infection rate,

bioRxiv preprint doi: https://doi.org/10.1101/2020.09.01.277764; this version posted September 1, 2020. The copyright holder for this preprint (which was not certified by peer review) is the author/funder. All rights reserved. No reuse allowed without permission.

HeLa cells infected with GFP-expressing *Salmonella* SL1344 as above were fixed in methanol and stained for TfR and LC3B. Z-stacks if images were acquired on an API Delta Vision Core microscope using the 20x lens and a spacing of 0.13 µm. A range of 5'000 – 18'000 cells/sample were imaged on 5-7 different areas on the coverslip, deconvoluted and stitched together on a SoftWoRx Imaging Workstastion. The final 3D pictures were analyzed with Fiji.

Yeast two-hybrid screen and interaction domain identification

The pB29-Rbpt5(1–862)-LexA bait plasmid was used to screen a random-primed HeLa cells_RP1 cDNA library cloned into the pP6-Gal4-AD plasmid using a high-throughput proprietary yeast two-hybrid-based technology (ULTImate Y2H Screen; Hybrigenics, Paris, France). To identify the FIP200 interaction segment in Rabaptin5, interaction domain mapping analysis of different fragments in pB29-Rbpt5(#)-LexA was performed with pP6-Gal4AD-FIP200(257–444) (Hybrigenics).

ACKNOWLEDGMENTS

We thank Drs. Mauricio Rosas Ballina and Dirk Bumann (Biozentrum) for materials and assistance with the *Salmonella* experiments, Drs. Kai Schleicher, Alexia Loynton-Ferrand and the Biozentrum Imaging Core Facility, and Janine Bögli of the FACS Core Facility for their support. This work was supported by Grant 31003A-182519 from the Swiss National Science Foundation.

AUTHOR CONTRIBUTIONS

VM, SS, SK planned and performed experiments and analyzed data. MS planned experiments and analyzed data. VM and MS wrote the manuscript.

CONFLICT OF INTEREST

The authors declare that they have no conflict of interest.

bioRxiv preprint doi: https://doi.org/10.1101/2020.09.01.277764; this version posted September 1, 2020. The copyright holder for this preprint (which was not certified by peer review) is the author/funder. All rights reserved. No reuse allowed without permission.

REFERENCES

Anding, A.L., and Baehrecke, E.H. (2017). Cleaning House: Selective Autophagy of Organelles. Dev Cell *41*, 10–22.

Bakula, D., Müller, A.J., Zuleger, T., Takacs, Z., Franz-Wachtel, M., Thost, A.-K., Brigger, D., Tschan, M.P., Frickey, T., Robenek, H., et al. (2017). WIPI3 and WIPI4 β-propellers are scaffolds for LKB1-AMPK-TSC signalling circuits in the control of autophagy. Nat Commun *8*, 15637.

Bento, C.F., Renna, M., Ghislat, G., Puri, C., Ashkenazi, A., Vicinanza, M., Menzies, F.M., and Rubinsztein, D.C. (2016). Mammalian Autophagy: How Does It Work? Annu Rev Biochem *85*, 685–713.

Birgisdottir, Å.B., and Johansen, T. (2020). Autophagy and endocytosis – interconnections and interdependencies. J Cell Sci *133*, jcs228114.

Boada-Romero, E., Letek, M., Fleischer, A., Pallauf, K., Ramón-Barros, C., and Pimentel-Muiños, F.X. (2013). TMEM59 defines a novel ATG16L1-binding motif that promotes local activation of LC3. Embo J *32*, 566–582.

Chauhan, S., Kumar, S., Jain, A., Ponpuak, M., Mudd, M.H., Kimura, T., Choi, S.W., Peters, R., Mandell, M., Bruun, J.-A., et al. (2016). TRIMs and Galectins Globally Cooperate and TRIM16 and Galectin-3 Co-direct Autophagy in Endomembrane Damage Homeostasis. Dev Cell *39*, 13–27.

Dikic, I., and Elazar, Z. (2018). Mechanism and medical implications of mammalian autophagy. Nat Rev Mol Cell Biol *19*, 349–364.

Dooley, H.C., Razi, M., Polson, H.E.J., Girardin, S.E., Wilson, M.I., and Tooze, S.A. (2014). WIPI2 links LC3 conjugation with PI3P, autophagosome formation, and pathogen clearance by recruiting Atg12-5-16L1. Mol Cell *55*, 238–252.

Dudley, L.J., Cabodevilla, A.G., Makar, A.N., Sztacho, M., Michelberger, T., Marsh, J.A., Houston, D.R., Martens, S., Jiang, X., and Gammoh, N. (2019). Intrinsic lipid binding activity of ATG16L1 supports efficient membrane anchoring and autophagy. Embo J *38*.

Dudley, L.J., Makar, A.N., and Gammoh, N. (2020). Membrane targeting of core autophagy players during autophagosome biogenesis. Febs J.

Fletcher, K., Ulferts, R., Jacquin, E., Veith, T., Gammoh, N., Arasteh, J.M., Mayer, U., Carding, S.R., Wileman, T., Beale, R., et al. (2018). The WD40 domain of ATG16L1 is required for its non-canonical role in lipidation of LC3 at single membranes. Embo J *37*, 24.

Florey, O., Gammoh, N., Kim, S.E., Jiang, X., and Overholtzer, M. (2015). V-ATPase and osmotic imbalances activate endolysosomal LC3 lipidation. Autophagy *11*, 88–99.

Fracchiolla, D., Chang, C., Hurley, J.H., and Martens, S. (2020). A PI3K-WIPI2 positive feedback loop allosterically activates LC3 lipidation in autophagy. J Cell Biol *219*.

Fujita, N., Morita, E., Itoh, T., Tanaka, A., Nakaoka, M., Osada, Y., Umemoto, T., Saitoh, T., Nakatogawa, H., Kobayashi, S., et al. (2013). Recruitment of the autophagic machinery to endosomes during infection is mediated by ubiquitin. *203*, 115–128.

Gammoh, N., Florey, O., Overholtzer, M., and Jiang, X. (2013). Interaction between FIP200 and ATG16L1 distinguishes ULK1 complex-dependent and -independent autophagy. Nat Struct Mol Biol *20*, 144–149.

bioRxiv preprint doi: https://doi.org/10.1101/2020.09.01.277764; this version posted September 1, 2020. The copyright holder for this preprint (which was not certified by peer review) is the author/funder. All rights reserved. No reuse allowed without permission.

Hara, T., Takamura, A., Kishi, C., Iemura, S.-I., Natsume, T., Guan, J.-L., and Mizushima, N. (2008). FIP200, a ULK-interacting protein, is required for autophagosome formation in mammalian cells. J Cell Biol *181*, 497–510.

Heckmann, B.L., and Green, D.R. (2019). LC3-associated phagocytosis at a glance. J Cell Sci *132*, jcs222984.

Heckmann, B.L., Boada-Romero, E., Cunha, L.D., Magne, J., and Green, D.R. (2017). LC3-Associated Phagocytosis and Inflammation. J. Mol. Biol. *429*, 3561–3576.

Heckmann, B.L., Teubner, B.J.W., Tummers, B., Boada-Romero, E., Harris, L., Yang, M., Guy, C.S., Zakharenko, S.S., and Green, D.R. (2019). LC3-Associated Endocytosis Facilitates β-Amyloid Clearance and Mitigates Neurodegeneration in Murine Alzheimer's Disease. Cell *178*, 536–551.e14.

Horiuchi, H., Lippé, R., McBride, H.M., Rubino, M., Woodman, P., Stenmark, H., Rybin, V., Wilm, M., Ashman, K., Mann, M., et al. (1997). A novel Rab5 GDP/GTP exchange factor complexed to Rabaptin-5 links nucleotide exchange to effector recruitment and function. Cell *90*, 1149–1159.

Huotari, J., and Helenius, A. (2011). Endosome maturation. Embo J *30*, 3481–3500.

Jacquin, E., Leclerc-Mercier, S., Judon, C., Blanchard, E., Fraitag, S., and Florey, O. (2017). Pharmacological modulators of autophagy activate a parallel noncanonical pathway driving unconventional LC3 lipidation. Autophagy *13*, 854–867.

Johansen, T., and Lamark, T. (2019). Selective Autophagy: ATG8 Family Proteins, LIR Motifs and Cargo Receptors. J. Mol. Biol.

Kageyama, S., Omori, H., Saitoh, T., Sone, T., Guan, J.-L., Akira, S., Imamoto, F., Noda, T., and Yoshimori, T. (2011). The LC3 recruitment mechanism is separate from Atg9L1-dependent membrane formation in the autophagic response against Salmonella. Mol Biol Cell *22*, 2290–2300.

Karanasios, E., Stapleton, E., Manifava, M., Kaizuka, T., Mizushima, N., Walker, S.A., and Ktistakis, N.T. (2013). Dynamic association of the ULK1 complex with omegasomes during autophagy induction. J Cell Sci *126*, 5224–5238.

Kälin, S., Buser, D.P., and Spiess, M. (2016). A fresh look at the function of Rabaptin5 on endosomes. Small GTPases *7*, 34–37.

Kälin, S., Hirschmann, D.T., Buser, D.P., and Spiess, M. (2015). Rabaptin5 is recruited to endosomes by Rab4 and Rabex5 to regulate endosome maturation. J Cell Sci *128*, 4126–4137.

Kimura, S., Noda, T., and Yoshimori, T. (2007). Dissection of the autophagosome maturation process by a novel reporter protein, tandem fluorescent-tagged LC3. Autophagy *3*, 452–460.

Kirkin, V., and Rogov, V.V. (2019). A Diversity of Selective Autophagy Receptors Determines the Specificity of the Autophagy Pathway. Mol Cell *76*, 268–285.

Kishi-Itakura, C., Ktistakis, N.T., and Buss, F. (2020). Ultrastructural insights into pathogen clearance by autophagy. Traffic *21*, 310–323.

Knævelsrud, H., Søreng, K., Raiborg, C., Håberg, K., Rasmuson, F., Brech, A., Liestøl, K., Rusten, T.E., Stenmark, H., Neufeld, T.P., et al. (2013). Membrane remodeling by the PX-BAR protein SNX18 promotes autophagosome formation. J Cell Biol *202*, 331–349.

bioRxiv preprint doi: https://doi.org/10.1101/2020.09.01.277764; this version posted September 1, 2020. The copyright holder for this preprint (which was not certified by peer review) is the author/funder. All rights reserved. No reuse allowed without permission.

Kumar, S., Chauhan, S., Jain, A., Ponpuak, M., Choi, S.W., Mudd, M., Peters, R., Mandell, M.A., Johansen, T., and Deretic, V. (2017). Galectins and TRIMs directly interact and orchestrate autophagic response to endomembrane damage. Autophagy *13*, 1086–1087.

LaRock, D.L., Chaudhary, A., and Miller, S.I. (2015). Salmonellae interactions with host processes. Nature Reviews Microbiology 2014 12:2 *13*, 191–205.

Leidal, A.M., Levine, B., and Debnath, J. (2018). Autophagy and the cell biology of age-related disease. Nat Cell Biol *20*, 1338–1348.

Levin, R., Grinstein, S., and Canton, J. (2016). The life cycle of phagosomes: formation, maturation, and resolution. Immunol. Rev. *273*, 156–179.

Lippé, R., Miaczynska, M., Rybin, V., Runge, A., and Zerial, M. (2001). Functional synergy between Rab5 effector Rabaptin-5 and exchange factor Rabex-5 when physically associated in a complex. Mol Biol Cell *12*, 2219–2228.

Lystad, A.H., Carlsson, S.R., la Ballina, de, L.R., Kauffman, K.J., Nag, S., Yoshimori, T., Melia, T.J., and Simonsen, A. (2019). Distinct functions of ATG16L1 isoforms in membrane binding and LC3B lipidation in autophagy-related processes. Nat Cell Biol *21*, 372–383.

Maejima, I., Takahashi, A., Omori, H., Kimura, T., Takabatake, Y., Saitoh, T., Yamamoto, A., Hamasaki, M., Noda, T., Isaka, Y., et al. (2013). Autophagy sequesters damaged lysosomes to control lysosomal biogenesis and kidney injury. Embo J *32*, 2336–2347.

Martinez, J., Almendinger, J., Oberst, A., Ness, R., Dillon, C.P., Fitzgerald, P., Hengartner, M.O., and Green, D.R. (2011). Microtubule-associated protein 1 light chain 3 alpha (LC3)-associated phagocytosis is required for the efficient clearance of dead cells. Proc. Natl. Acad. Sci. U.S.a. *108*, 17396–17401.

Martinez, J., Malireddi, R.K.S., Lu, Q., Cunha, L.D., Pelletier, S., Gingras, S., Orchard, R., Guan, J.-L., Tan, H., Peng, J., et al. (2015). Molecular characterization of LC3-associated phagocytosis reveals distinct roles for Rubicon, NOX2 and autophagy proteins. Nat Cell Biol *17*, 893–906.

Mattera, R., and Bonifacino, J.S. (2008). Ubiquitin binding and conjugation regulate the recruitment of Rabex-5 to early endosomes. Embo J *27*, 2484–2494.

Mattera, R., Tsai, Y.C., Weissman, A.M., and Bonifacino, J.S. (2006). The Rab5 guanine nucleotide exchange factor Rabex-5 binds ubiquitin (Ub) and functions as a Ub ligase through an atypical Ub-interacting motif and a zinc finger domain. J Biol Chem *281*, 6874–6883.

Mauthe, M., Orhon, I., Rocchi, C., Zhou, X., Luhr, M., Hijlkema, K.-J., Coppes, R.P., Engedal, N., Mari, M., and Reggiori, F. (2018). Chloroquine inhibits autophagic flux by decreasing autophagosome-lysosome fusion. Autophagy *14*, 1435–1455.

Mercer, T.J., Gubas, A., and Tooze, S.A. (2018). A Molecular Perspective of Mammalian Autophagosome Biogenesis. J Biol Chem *293*, 5386–5395.

Morishita, H., and Mizushima, N. (2019). Diverse Cellular Roles of Autophagy. Annu Rev Cell Dev Biol *35*, 453–475.

Naslavsky, N., and Caplan, S. (2018). The enigmatic endosome – sorting the ins and outs of endocytic trafficking. J Cell Sci *131*, jcs216499.

bioRxiv preprint doi: https://doi.org/10.1101/2020.09.01.277764; this version posted September 1, 2020. The copyright holder for this preprint (which was not certified by peer review) is the author/funder. All rights reserved. No reuse allowed without permission.

Papadopoulos, C., Kirchner, P., Bug, M., Grum, D., Koerver, L., Schulze, N., Poehler, R., Dressler, A., Fengler, S., Arhzaouy, K., et al. (2017). VCP/p97 cooperates with YOD1, UBXD1 and PLAA to drive clearance of ruptured lysosomes by autophagy. Embo J *36*, 135–150.

Popovic, D., and Dikic, I. (2014). TBC1D5 and the AP2 complex regulate ATG9 trafficking and initiation of autophagy. EMBO Rep *15*, 392–401.

Poteryaev, D., Datta, S., Ackema, K., Zerial, M., and Spang, A. (2010). Identification of the switch in early-to-late endosome transition. Cell *141*, 497–508.

Puri, C., Renna, M., Bento, C.F., Moreau, K., and Rubinsztein, D.C. (2013). Diverse autophagosome membrane sources coalesce in recycling endosomes. Cell *154*, 1285–1299.

Puri, C., Vicinanza, M., Ashkenazi, A., Gratian, M.J., Zhang, Q., Bento, C.F., Renna, M., Menzies, F.M., and Rubinsztein, D.C. (2018). The RAB11A-Positive Compartment Is a Primary Platform for Autophagosome Assembly Mediated by WIPI2 Recognition of PI3P-RAB11A. Dev Cell *45*, 114–131.e118.

Ran, F.A., Hsu, P.D., Wright, J., Agarwala, V., Scott, D.A., and Zhang, F. (2013). Genome engineering using the CRISPR-Cas9 system. Nat Protoc *8*, 2281–2308.

Shi, X., Yokom, A.L., Wang, C., Young, L.N., Youle, R.J., and Hurley, J.H. (2020). ULK complex organization in autophagy by a C-shaped FIP200 N-terminal domain dimer. J Cell Biol *219*.

Steele-Mortimer, O., Méresse, S., Gorvel, J.P., Toh, B.H., and Finlay, B.B. (1999). Biogenesis of Salmonella typhimurium-containing vacuoles in epithelial cells involves interactions with the early endocytic pathway. Cell. Microbiol. *1*, 33–49.

Thurston, T.L.M., Wandel, M.P., Muhlinen, von, N., Foeglein, A., and Randow, F. (2012). Galectin 8 targets damaged vesicles for autophagy to defend cells against bacterial invasion. Nature *482*, 414–418.

Turco, E., Witt, M., Abert, C., Bock-Bierbaum, T., Su, M.-Y., Trapannone, R., Sztacho, M., Danieli, A., Shi, X., Zaffagnini, G., et al. (2019). FIP200 Claw Domain Binding to p62 Promotes Autophagosome Formation at Ubiquitin Condensates. Mol Cell *74*, 330–346.e11.

Vargas, J.N.S., Wang, C., Bunker, E., Hao, L., Maric, D., Schiavo, G., Randow, F., and Youle, R.J. (2019). Spatiotemporal Control of ULK1 Activation by NDP52 and TBK1 during Selective Autophagy. Mol Cell *74*, 347–362.e6.

Zhang, Z., Zhang, T., Wang, S., Gong, Z., Tang, C., Chen, J., and Ding, J. (2014). Molecular mechanism for Rabex-5 GEF activation by Rabaptin-5. Elife *3*, e02687–e02687.

Zheng, Y.T., Shahnazari, S., Brech, A., Lamark, T., Johansen, T., and Brumell, J.H. (2009). The adaptor protein p62/SQSTM1 targets invading bacteria to the autophagy pathway. J. Immunol. *183*, 5909–5916.

Zhu, G., Zhai, P., He, X., Wakeham, N., Rodgers, K., Li, G., Tang, J., and Zhang, X.C. (2004). Crystal structure of human GGA1 GAT domain complexed with the GAT-binding domain of Rabaptin5. Embo J *23*, 3909–3917.

bioRxiv preprint doi: https://doi.org/10.1101/2020.09.01.277764; this version posted September 1, 2020. The copyright holder for this preprint (which was not certified by peer review) is the author/funder. All rights reserved. No reuse allowed without permission.

FIGURES

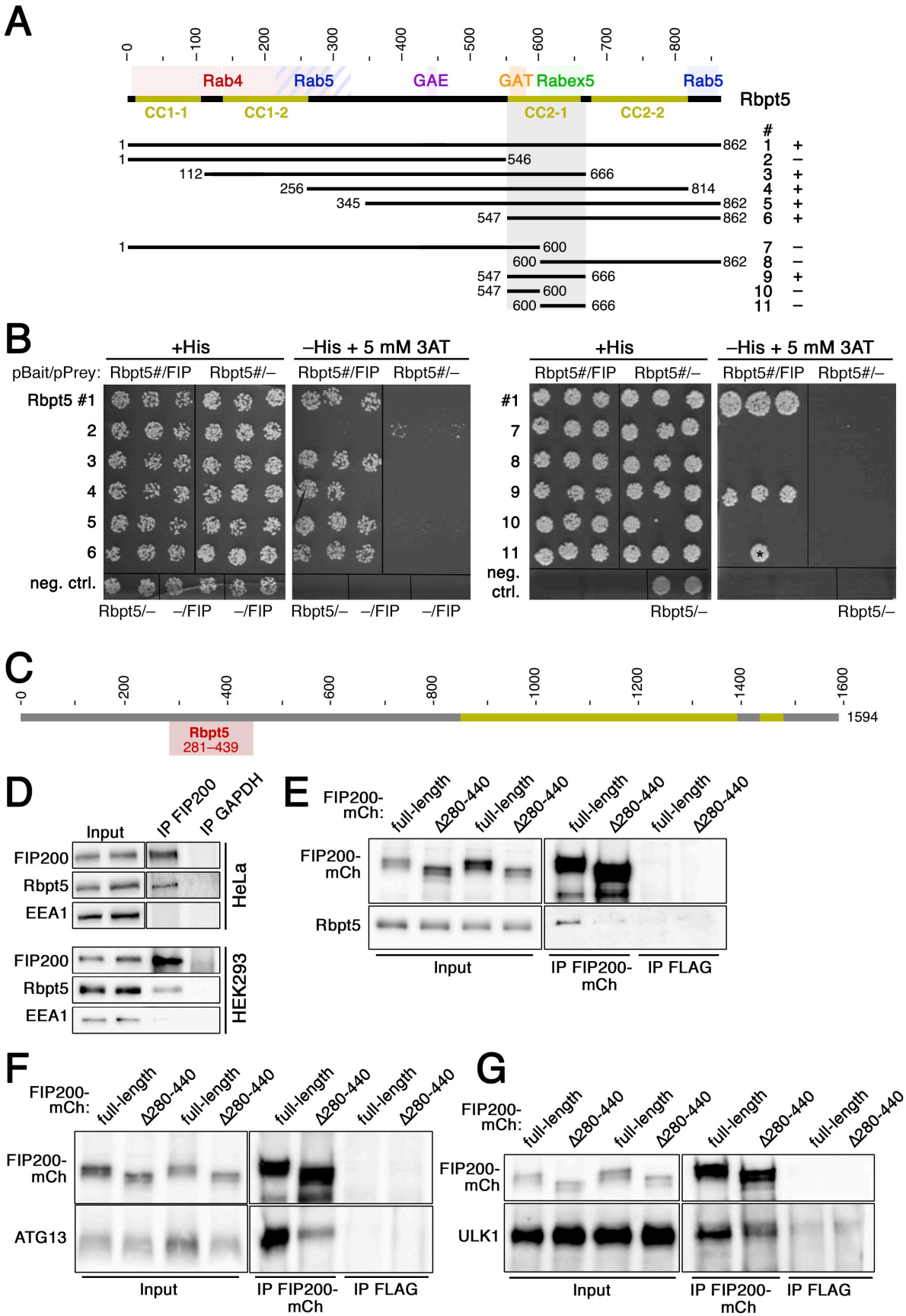

bioRxiv preprint doi: https://doi.org/10.1101/2020.09.01.277764; this version posted September 1, 2020. The copyright holder for this preprint (which was not certified by peer review) is the author/funder. All rights reserved. No reuse allowed without permission.

Figure 1. Interaction of Rabaptin5 with FIP200 as identified by two-hybrid analysis in yeast and by co-immunoprecipitation in HeLa and HEK293A cells.

A: Schematic representation of the sequence of Rabaptin5. Coiled-coil (CC) segments are shown in yellow. Colored backgrounds highlight the segments shown to interact with Rab4, Rab5, Rabex5, and the GAE and GAT domains of GGAs (Golgi-localizing, γ-adaptin ear homology domain, ARF-binding proteins). Below, the segments used to test yeast two-hybrid interaction with residues 257–444 of FIP200 are shown with their number (#) and the observed interaction (+ or –).

B: Yeast two-hybrid analysis for interaction between the above-shown Rabaptin5 segments (Rbpt5#, fused to LexA on the bait plasmid) and residues 257–444 of FIP200 (FIP, fused to the Gal4 activation domain on the prey plasmid) to drive HIS3 expression. Three different clones each were replica-plated on medium with His or without His, but containing 3-amino-1,2,4-triazole (3AT; an inhibitor of His synthesis to increase stringency) and grown in the absence of Trp and leucine as a control. As negative controls, empty bait or prey plasmids were used. The asterisk indicates a clone invalidated by recombination.

C: Schematic representation of the sequence of FIP200 with its coiled coil segments in yellow. Residues 281–439 (gray) indicates the minimal sequence identified to interact with Rabaptin5 in the yeast two-hybrid screen.

D: FIP200 was immunoprecipitated (IP) from lysates of HeLa or HEK293A cells and probed for FIP200, Rabaptin5 (Rbpt5), and EEA1 (early endosome antigen 1) by immunoblotting. Input lysate (10%) was immunoblotted blotted parallel. As a negative control, the immunoprecipitation was performed using an anti-GAPDH antibody.

E–G: Lysates of HeLa cells transiently transfected with full-length FIP200-mCherry (FIP200-mCh) or a deletion mutant lacking the segment interacting with Rabaptin5 (Δ280–440) were immuprecipitated with anti -mCherry (IP FIP200-mCh) or, as a control, with anti-FLAG antibodies (IP FLAG). Immunoprecipitates and input lysates (10%) were immunoblotted for mCherry and Rabaptin5 (E), ATG13 (F), or ULK1 (G).

bioRxiv preprint doi: https://doi.org/10.1101/2020.09.01.277764; this version posted September 1, 2020. The copyright holder for this preprint (which was not certified by peer review) is the author/funder. All rights reserved. No reuse allowed without permission.

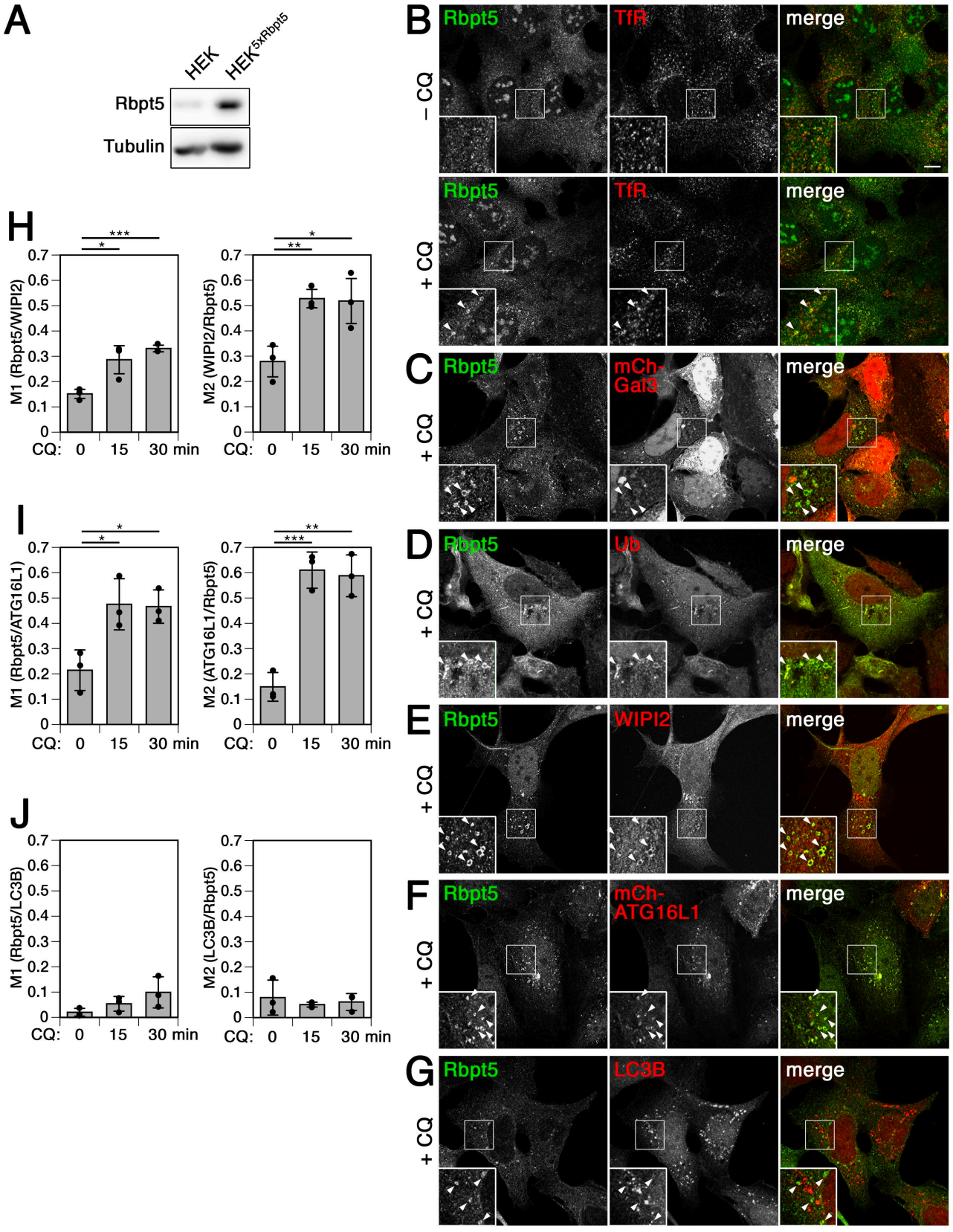

Figure 2. Chloroquine treatment induces autophagy of Rabaptin5-positive endosomes.
A: Immunoblot of Rabaptin5 levels in wild-type HEK293A cells and stable HEK^{+Rbpt5} cells overexpressing Rabaptin5.

bioRxiv preprint doi: https://doi.org/10.1101/2020.09.01.277764; this version posted September 1, 2020. The copyright holder for this preprint (which was not certified by peer review) is the author/funder. All rights reserved. No reuse allowed without permission.

B–G: HEK^{+Rbpt5} cells, untransfected or 24 h after transfection with mCherry-Galectin3 or mCherry-ATG16L1, without (–CQ) or with chloroquine treatment (60 µM) for 30 min (+CQ), were analyzed by immunofluorescence microscopy for Rabaptin5 and either transferrin receptor (TfR) (B), mCherry-Galectin3 (C), ubiquitin (D), WIPI2 (E), mCherry-ATG16L1 (F), or LC3B (G). In the enlarged insets, arrowheads point out chloroquine-induced enlarged early (circular) endosomes. Bar, 10 µm.
H–J: HEK^{+Rbpt5} cells, untransfected or 24 h after transfection with mCherry-ATG16L1, were treated with 60 µM chloroquine for 0, 15 and 30 min and stained for Rabaptin5 and either WIPI2, mCherry-ATG16L1, or LC3B. Mander's colocalization coefficients were determined, M1 showing the fraction of Rabaptin5-positive structures also positive for WIPI2 (H), mCherry-ATG16L1 (I), or LC3B (J), and M2 showing the respective inverse (mean and standard deviation of three independent experiments; two-tailed Student's t test: *$p < 0.05$, **$p < 0.01$, ***$p<0.001$).

bioRxiv preprint doi: https://doi.org/10.1101/2020.09.01.277764; this version posted September 1, 2020. The copyright holder for this preprint (which was not certified by peer review) is the author/funder. All rights reserved. No reuse allowed without permission.

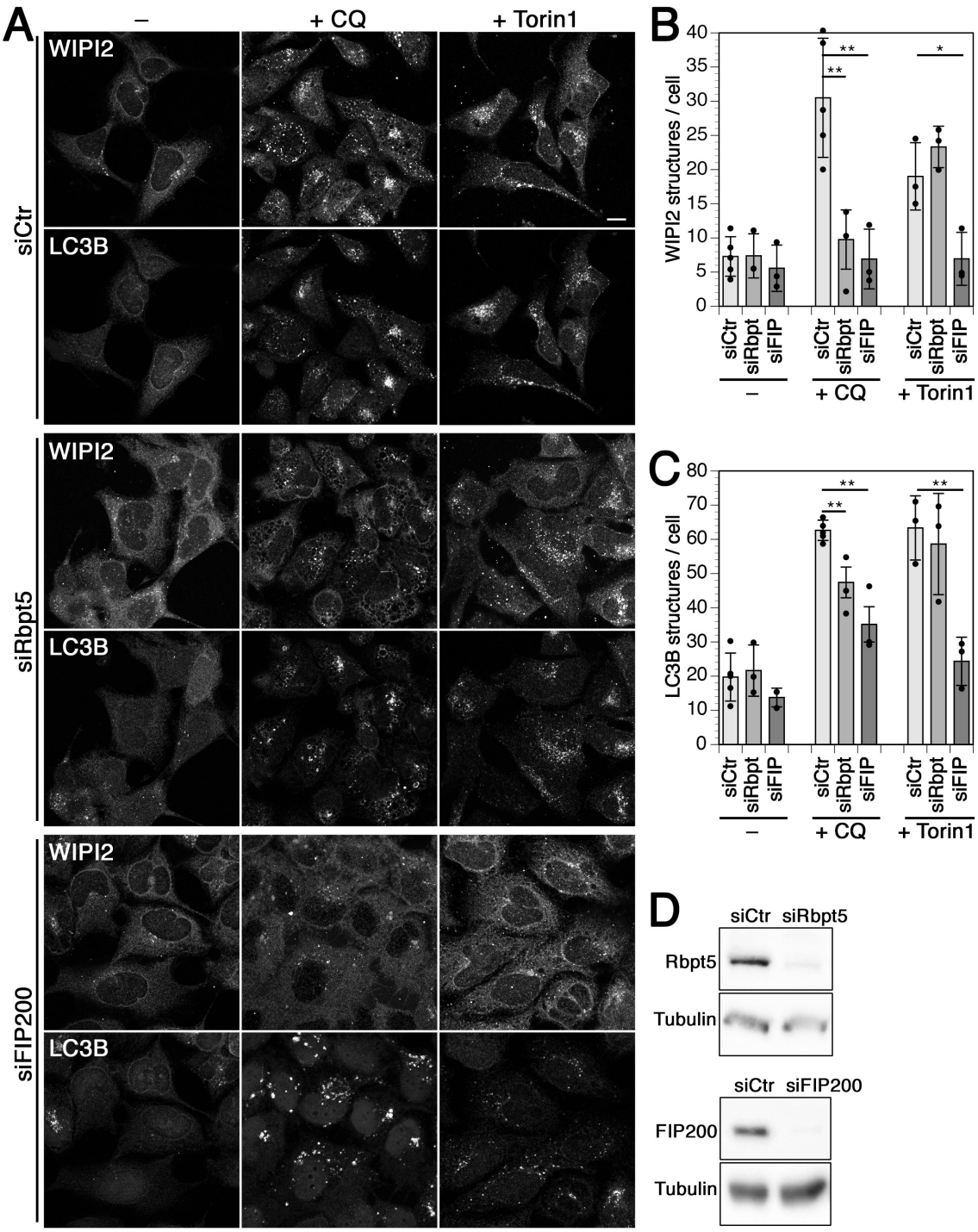

Figure 3. Chloroquine-, but not Torin1-induced autophagy depends on Rabaptin5.
A: HEK293A cells were transfected with nontargeting siRNA (siCtr) or siRNAs silencing Rabaptin5 (siRbpt5) or FIP200 (siFIP200) for 72 h and treated without (–) or with 60 µM chloroquine (+CQ) or 250 nM Torin1 for 150 min. Cells were fixed and immunostained for endogenous WIPI2 and LC3B. Bar, 10 µm.
B and C: WIPI2 (B) orLC3B puncta per cell (C) were quantified for each condition (mean and standard deviation of three independent experiments; two-tailed Student's t test: *p < 0.05, **p < 0.01, ***p<0.001).
D: Efficiency of Rabaptin5 and FIP200 knockdown was assayed by immunoblotting.

bioRxiv preprint doi: https://doi.org/10.1101/2020.09.01.277764; this version posted September 1, 2020. The copyright holder for this preprint (which was not certified by peer review) is the author/funder. All rights reserved. No reuse allowed without permission.

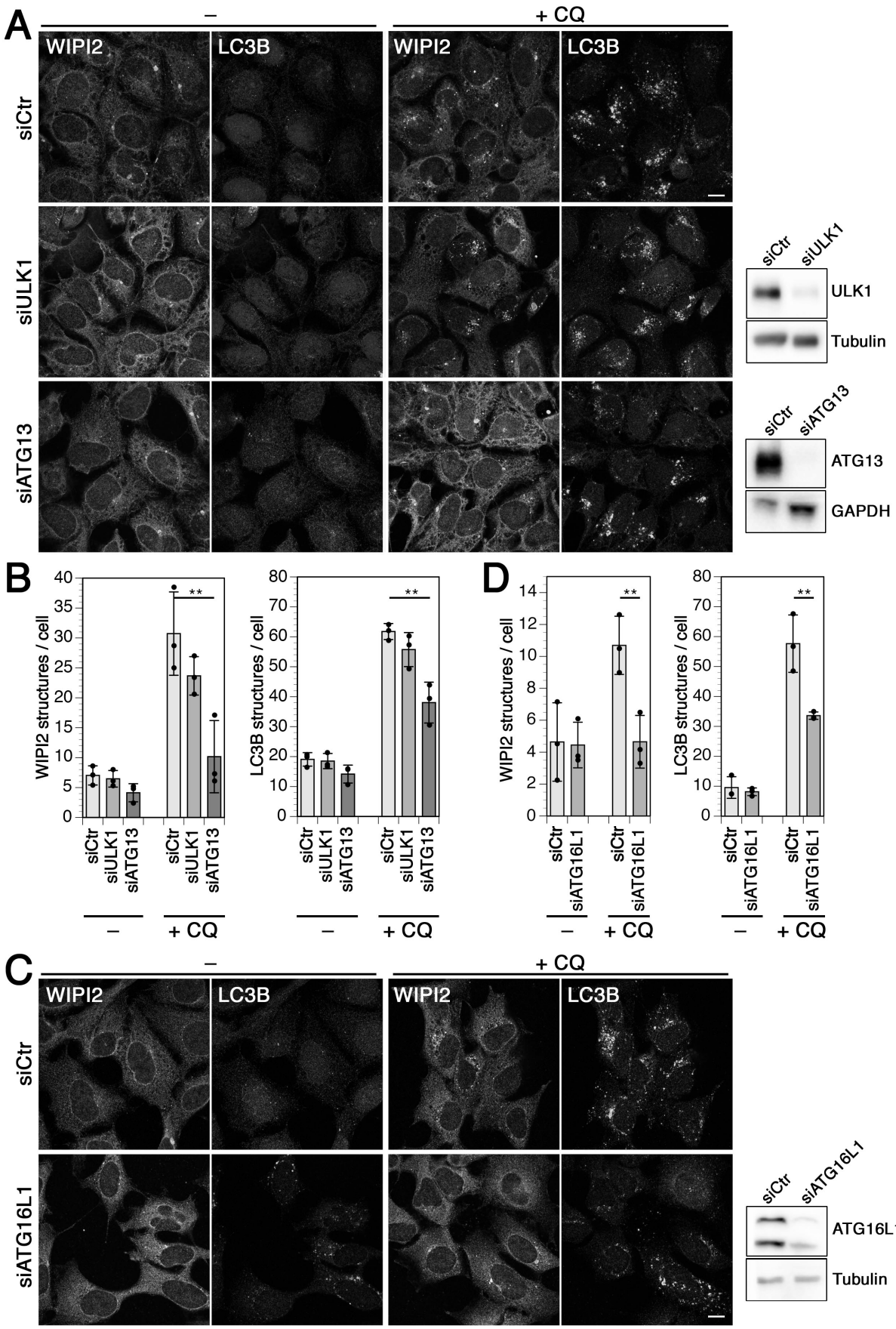

bioRxiv preprint doi: https://doi.org/10.1101/2020.09.01.277764; this version posted September 1, 2020. The copyright holder for this preprint (which was not certified by peer review) is the author/funder. All rights reserved. No reuse allowed without permission.

Figure 4. Chloroquine-induced endosomal autophagy requires ATG13 and ATG16L1, but not ULK1.
A: HEK293A cells were transfected with nontargeting siRNA (siCtr) or siRNAs silencing ULK1 (siULK1) or ATG13 (siATG13) for 72 h, treated without (–) or with 60 μM chloroquine (+CQ) for 150 minutes, and fixed and immunostained for endogenous WIPI2 and LC3B. Bar, 10 μm. Efficiency of ULK1 and ATG13 knockdown was assayed by immunoblotting on the right.
B: WIPI2 of LC3B puncta per cell were quantified for each condition (mean and standard deviation of three independent experiments; two-tailed Student's t test: *$p < 0.05$, **$p < 0.01$).
C: Cells were transfected with control siRNA or siRNA silencing ATG16L1, treated for 150 min with chloroquine as in (A), and fixed and stained for WIPI2 and LC3B. Bar, 10 μm. Efficiency of ATG16L1 knockdown was assayed by immunoblotting on the right.
D: WIPI2 of LC3B puncta per cell were quantified for each condition as in (B).

bioRxiv preprint doi: https://doi.org/10.1101/2020.09.01.277764; this version posted September 1, 2020. The copyright holder for this preprint (which was not certified by peer review) is the author/funder. All rights reserved. No reuse allowed without permission.

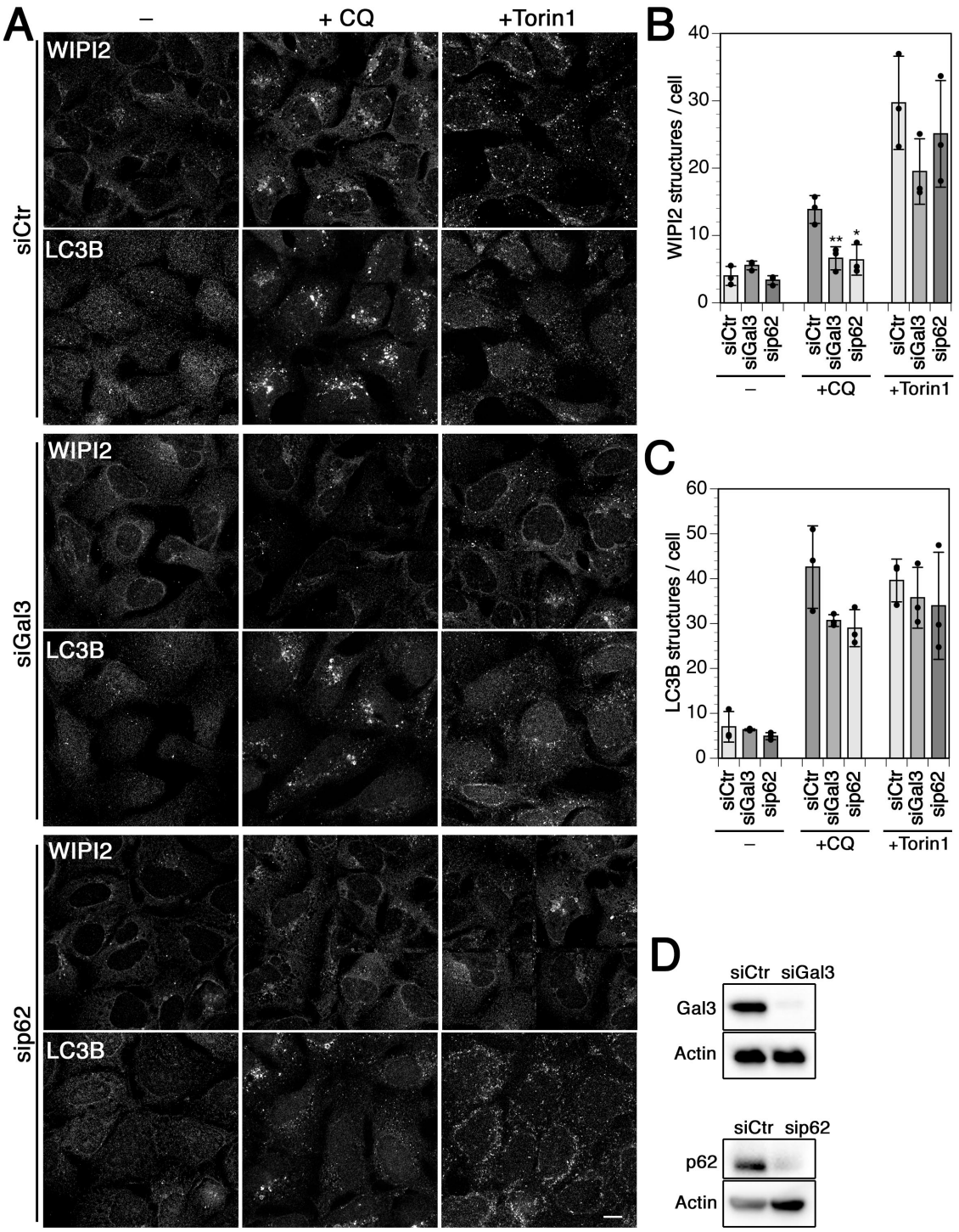

Figure 5. Chloroquine-induced autophagy involves galectin3 and p62.
A: HEK293A cells were transfected with nontargeting siRNA (siCtr) or siRNAs silencing galectin3 (siGal3) or p62 (sip62) for 72 h and treated without (–) or with 60 µM chloroquine (+CQ) or 250 nM Torin1 for 150 min. Cells were fixed and immunostained for endogenous WIPI2 and LC3B. Bar, 10 µm.
B and C: WIPI2 (B) or LC3B puncta per cell (C) were quantified for each condition (mean and standard deviation of three independent experiments; two-tailed Student's t test: *p < 0.05, **p < 0.01, ***p<0.001).
D: Efficiency of galectin3 and p62 knockdown was assayed by immunoblotting.

bioRxiv preprint doi: https://doi.org/10.1101/2020.09.01.277764; this version posted September 1, 2020. The copyright holder for this preprint (which was not certified by peer review) is the author/funder. All rights reserved. No reuse allowed without permission.

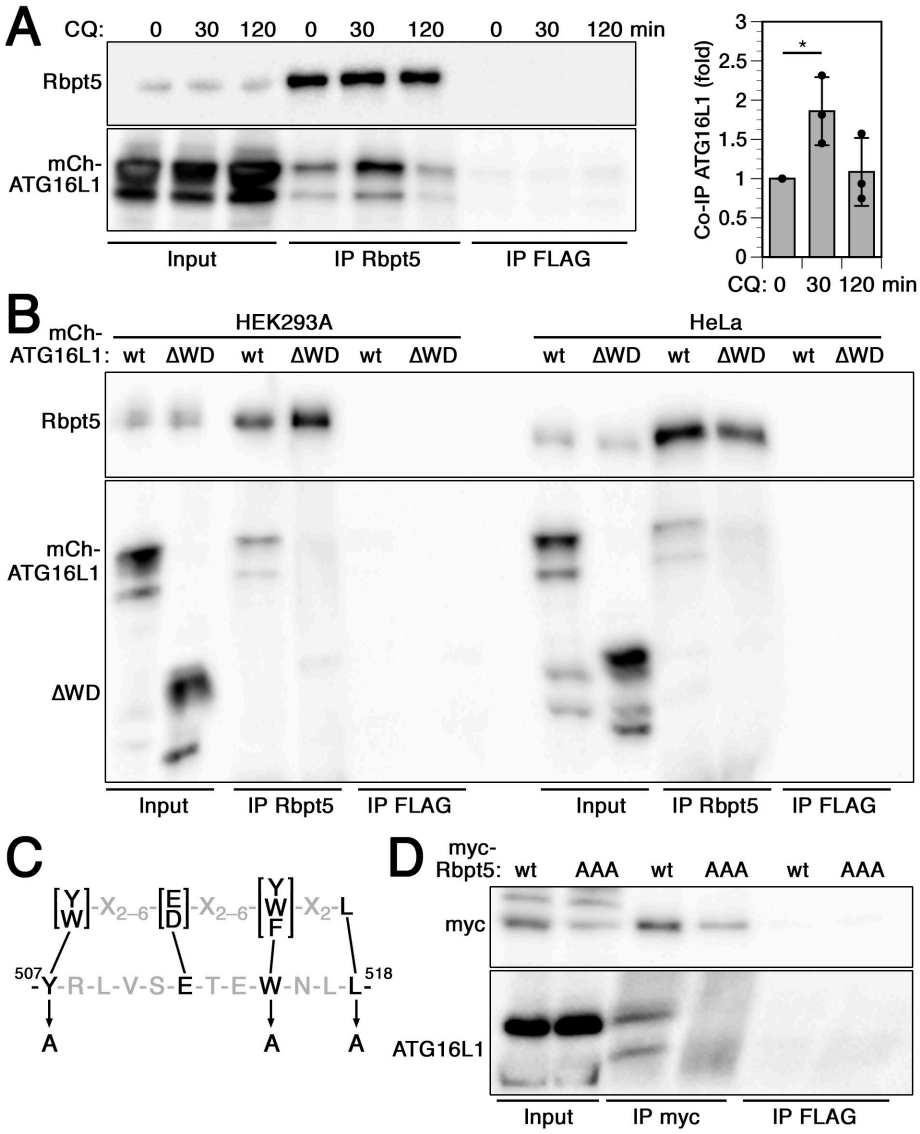

Figure 6. Rabaptin5 binds to the WD domain of ATG16L1 via a conserved interaction motif.
A: HeLa cells transiently transfected with full-length mCherry-ATG16L1 were treated with 60 µM chloroquine for 0, 30, or 120 min, lysed, and immunoprecipitated with anti-Rabaptin5 (IP: Rbpt5) or, as a control, with anti-FLAG antibodies (IP FLAG). Immunoprecipitates and input lysates (10%) were immunoblotted for Rabaptin5 and ATG16L1. Signals were quantified and the ratios of mCherry-ATG16L1/Rabaptin5 normalized to that without (0 min) chloroquine treatment (mean and standard deviation of three independent experiments; two-tailed Student's t test: *$p < 0.05$).
B: Lysates of HEK293A or HeLa cells transiently transfected with full-length mCherry-ATG16L1 (wt) or a mutant lacking the WD domain (ΔWD) were immunoprecipitated with anti-Rabaptin5 or anti-FLAG antibodies, and immunoblotted for Rabaptin5 and ATG16L1.
C: The consensus sequence of the ATG16L1 interaction motifs of TMEM59, NOD2, and TLR2 (above; Boada-Romero et al. 2013) is shown together with the matching sequence in Rabaptin5 (below). The three point mutations to alanine to produce the AAA mutant of Rabaptin5 are indicated.
D: Lysates of HeLa cells transiently transfected with myc-tagged wild-type Rabaptin5 (wt) or triple-alanine mutant (AAA) were immunoprecipitated with anti-myc (IP myc) or anti-FLAG antibodies (IP FLAG), and immunoblotted for myc and ATG16L1.

bioRxiv preprint doi: https://doi.org/10.1101/2020.09.01.277764; this version posted September 1, 2020. The copyright holder for this preprint (which was not certified by peer review) is the author/funder. All rights reserved. No reuse allowed without permission.

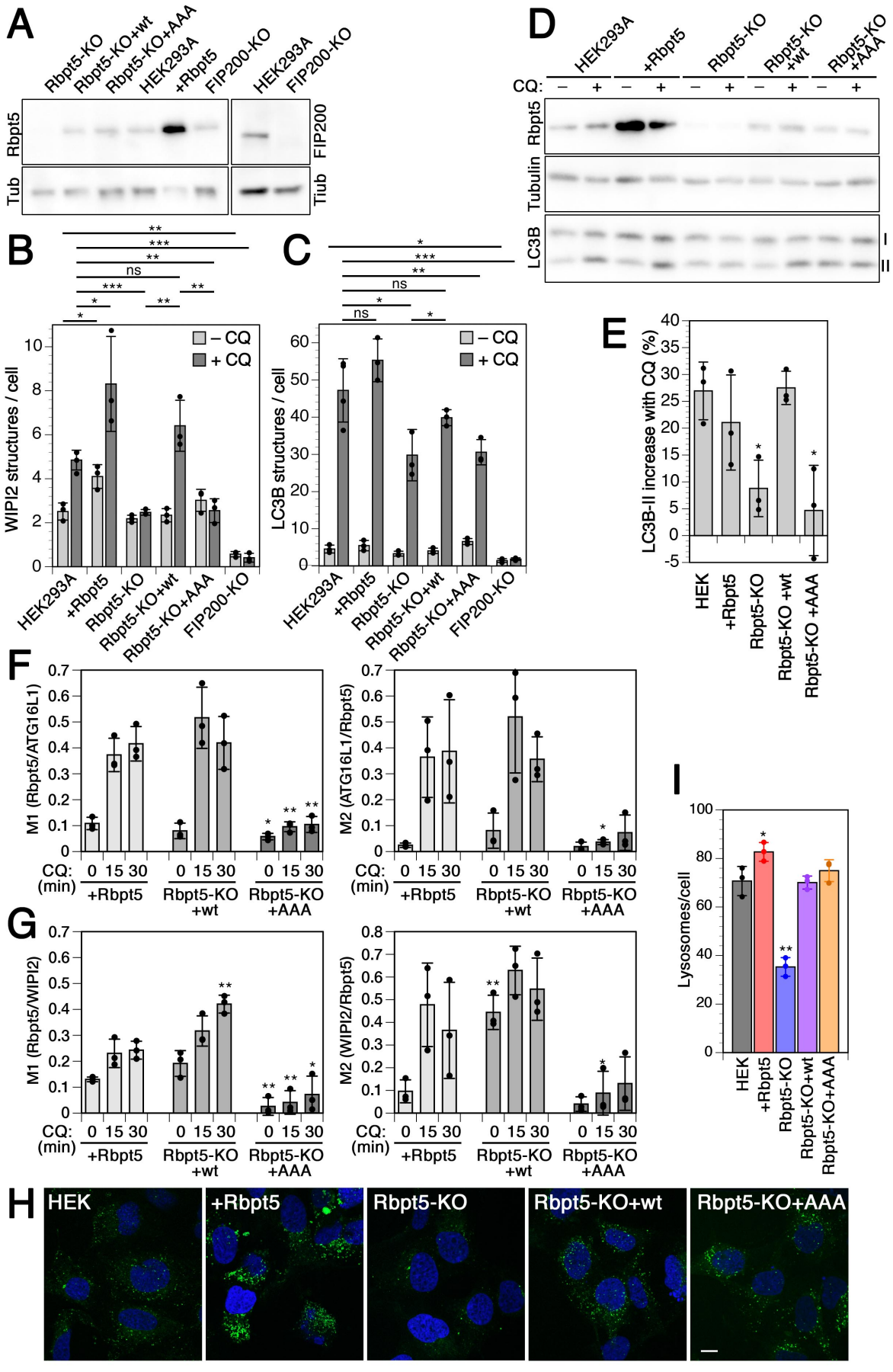

bioRxiv preprint doi: https://doi.org/10.1101/2020.09.01.277764; this version posted September 1, 2020. The copyright holder for this preprint (which was not certified by peer review) is the author/funder. All rights reserved. No reuse allowed without permission.

Figure 7. Chloroquine-induced endosomal autophagy depends on Rabaptin5 and its ATG16L1 binding motif.

A: By immunoblot analysis, the levels of Rabaptin5 and as a loading control of tubulin (Tub) were assessed in wild-type HEK293A cells, HEK^{+Rbpt5} cells stably overexpressing Rabaptin5, Rabaptin5-knockout cells without (Rbpt5-KO) or with stable re-expression of wild-type (Rbpt5-KO+wt) or AAA-mutant Rabaptin5 (Rbpt5-KO+AAA), and FIP200-knockout cells. On the right, FIP200 was blotted in HEK293A and FIP200-knockout cells.

B and **C**: The same stable HEK293A-derived cell lines were treated without (–CQ) or with 60 µM chloroquine for 150 min (+CQ)and analyzed by immunofluorescence microscopy for WIPI2 or LC3B as shown in Suppl. Figure S4. WIPI2 (B) of LC3B (C) puncta per cell were quantified for each condition (mean and standard deviation of three independent experiments; two-tailed Student's t test: *p < 0.05, **p < 0.01, ***p<0.001).

D and E: The HEK293A-derived cell lines were treated with 60 µM chloroquine for 30min and non-lipidated and lipidated LC3B (I and II, resp.) were assayed by immunoblot analysis (D). The increase of the LC3B-II fraction of total LC3B upon chloroquine treatment was quantified (mean and standard deviation of three independent experiments; two-tailed Student's t test: *p < 0.05).

F: HEK^{+Rbpt5} cells and Rabaptin5-knockout cells stably re-expressing wild-type (Rbpt5-KO+wt) or AAA-mutant Rabaptin5 (Rbpt5-KO+AAA) were transfected with mCherry-ATG16L1, treated with 60 µM chloroquine (CQ) for 0, 15 and 30 min, and analyzed by immunofluorescence microscopy for Rabaptin5 and mCherry-ATG16L1. Mander's colocalization coefficients were determined, M1 showing the fraction of Rabaptin5-positive structures also positive for mCherry-ATG16L1 and M2 showing the inverse (mean and standard deviation of three independent experiments; two-tailed Student's t test for Rbpt5-KO+AAA vs. HEK^{+Rbpt5} cells: *p < 0.05, **p < 0.01).

G: The same three cell lines as in panel D, but untransfected, were analyzed in the same way for Rabaptin5 and WIPI2.

H: Wild-type HEK293A cells, HEK^{+Rbpt5} cells, Rabaptin5-knockout cells without (Rbpt5-KO) or with stable re-expression of wild-type (Rbpt5-KO+wt) or AAA-mutant Rabaptin5 (Rbpt5-KO+AAA) were stained with lysotracker and with DAPI for nuclei. Bar, 10 µm.

I: The number of lysosomes (lysotracker-positive structures) per cell was quantified from cells as in panel C (mean and standard deviation of three independent experiments). Images for at least 15 cells per sample were quantified. The value for HEK^{+Rbpt5} cells is an underestimate, because the density of puncta makes them difficult to distinguish as separate structures.

bioRxiv preprint doi: https://doi.org/10.1101/2020.09.01.277764; this version posted September 1, 2020. The copyright holder for this preprint (which was not certified by peer review) is the author/funder. All rights reserved. No reuse allowed without permission.

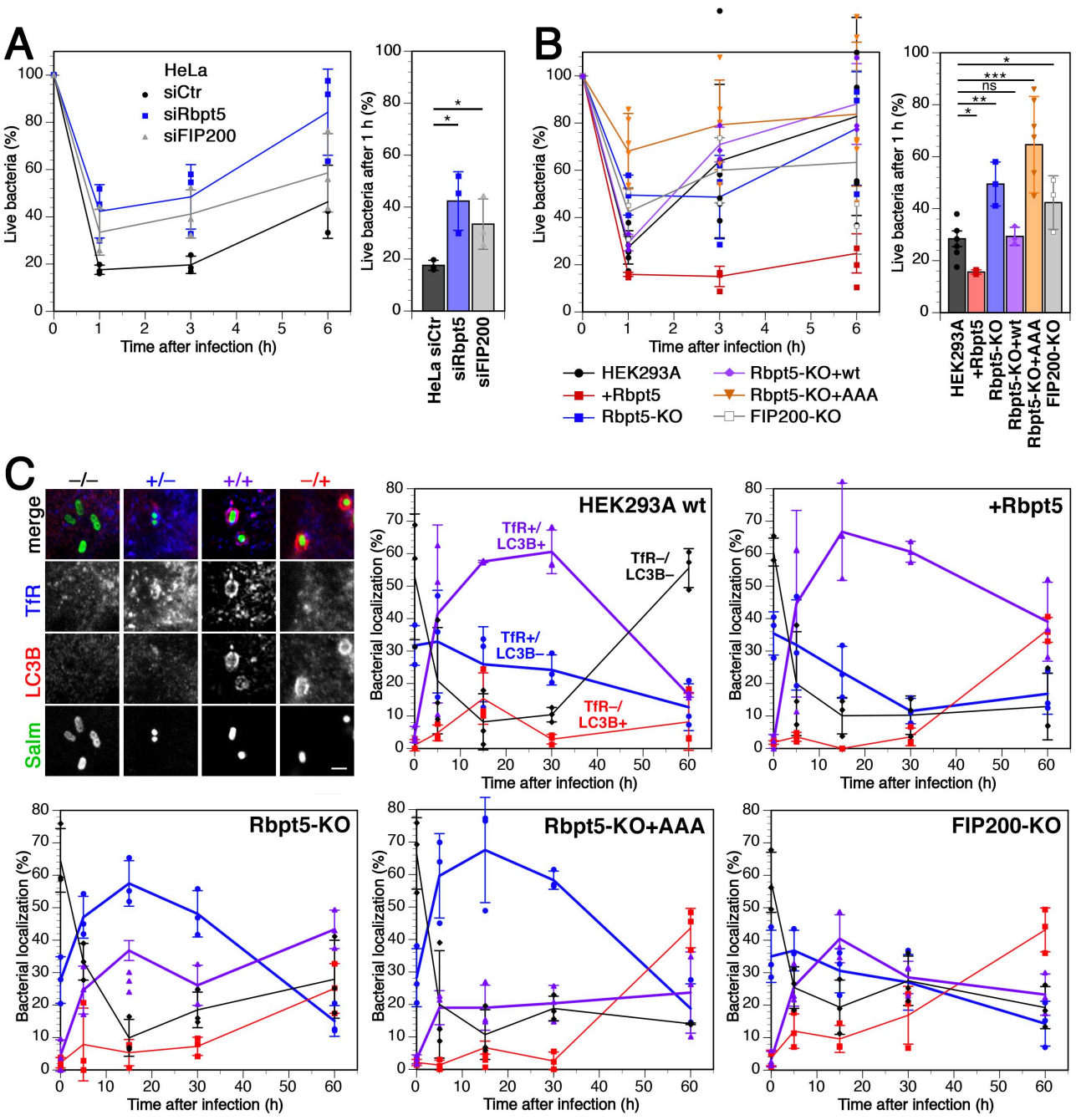

Figure 8 Rabaptin5-mediated autophagy contributes to early killing of *Salmonella*.
A: HeLa cells were transfected with nontargeting siRNA (siCtr) or siRNAs silencing Rabaptin5 (siRbpt5) or FIP200 (siFIP200) for 72 h. The cells were infected with *Salmonella* by centrifugation at 500×g for 5min at 37°C and incubation for 10 min at 37°C, washed three times, and incubated in fresh culture medium containing gentamicin to prevent growth of extracellular bacteria for 0, 1, 3, or 6 h before lysis of the host cells and plating of the bacteria on LB agar plates at various dilutions to determine the number of live bacteria at the different time points, shown as a percentage of internalized cells after infection (mean and standard deviation of three independent experiments). On the right, the fractions of internalized bacteria alive 1 h after infection are shown separately (mean and standard deviation of three independent experiments; two-tailed Student's t test: *p < 0.05).
B: Wild-type HEK293A, HEK^{+Rbpt5}, Rbpt5-KO, Rbpt5-KO+wt, Rbpt5-KO+AAA, and FIP200-KO cells were infected with *Salmonella* and treated and analyzed as in panels A (mean and standard deviation of three independent experiments; two-tailed Student's t test: *p < 0.05, **p < 0.01, ***p<0.001).

bioRxiv preprint doi: https://doi.org/10.1101/2020.09.01.277764; this version posted September 1, 2020. The copyright holder for this preprint (which was not certified by peer review) is the author/funder. All rights reserved. No reuse allowed without permission.

C: Wild-type HEK293A, HEK^{+Rbpt5}, Rbpt5-KO, Rbpt5-KO+AAA, and FIP200-KO cells were infected with *Salmonella* expressing GFP as in panel B, incubated in fresh culture medium containing gentamicin for 0, 5, 15, 30, and 60 min, fixed with methanol and immunostained for transferrin receptor (TfR) as a marker of early endosomes and for LC3B as a marker of autophagy. *Salmonella* were classified according to their association with a TfR- and/or LC3B-positive compartment – as illustrated on the top left (bar, 2 μm) – during the first hour after infection. In the absence of Rabaptin5, LC3-positive SCVs with early endosomal characteristics (containing TfR) were strongly reduced. (Means and standard deviations of three independent experiments, analyzing >50 bacteria for each time point.)

bioRxiv preprint doi: https://doi.org/10.1101/2020.09.01.277764; this version posted September 1, 2020. The copyright holder for this preprint (which was not certified by peer review) is the author/funder. All rights reserved. No reuse allowed without permission.

SUPPLEMENTARY INFORMATION

Suppl. Table S1. Rabaptin5 interactors identified by yeast two-hybrid screen.

Interaction quality*	Gene name	Protein	Interacting fragment
A	RABEP1	Rabaptin5	579–691
A	**RB1CC1**	**FIP200**	**281–439**
A	VIM	Vimentin	15–144
B	RABGEF1	Rabex5	281–439
B	BARD1	BRCA1-associated ring domain protein 1	47–284
B	GOLGA4	Golgin A4	1116–1281
B	ITSN1	Intersectin 1	554–667
C	SMARCC1	SWI/SNF complex subunit SMARCC1	899–1005

*A–C indicate the confidence level of the interaction from very high to medium.
FIP200, FAK family-interacting protein of 200 kDa; RB1CC1, RB1-inducible coiled-coil protein 1.

bioRxiv preprint doi: https://doi.org/10.1101/2020.09.01.277764; this version posted September 1, 2020. The copyright holder for this preprint (which was not certified by peer review) is the author/funder. All rights reserved. No reuse allowed without permission.

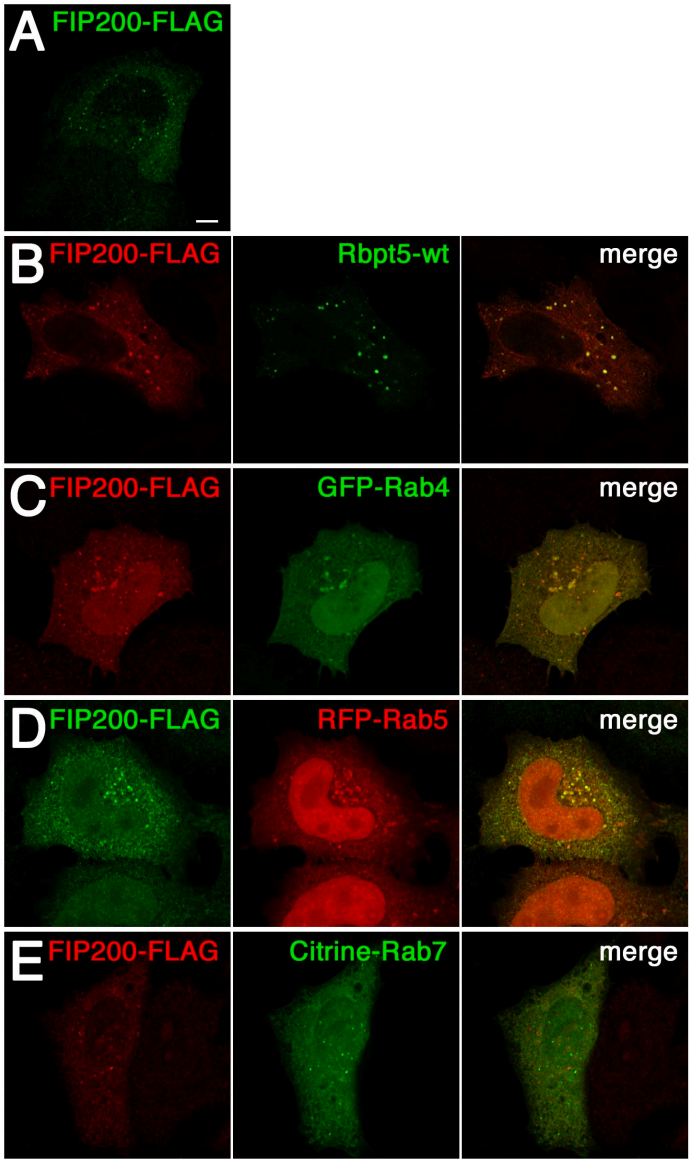

Suppl. Figure S1. FIP200 colocalizes with endosomal markers.
HeLa cells were transfected with FLAG-tagged FIP200 alone (A) or together with Rabaptin5 (Rbpt5-wt) (B), GFP-Rab4 (C), RFP-Rab5 (D), or Citrine-Rab7 (E), fixed after 24 h, and subjected to immunofluorescence microscopy. Bar, 10 μm.

bioRxiv preprint doi: https://doi.org/10.1101/2020.09.01.277764; this version posted September 1, 2020. The copyright holder for this preprint (which was not certified by peer review) is the author/funder. All rights reserved. No reuse allowed without permission.

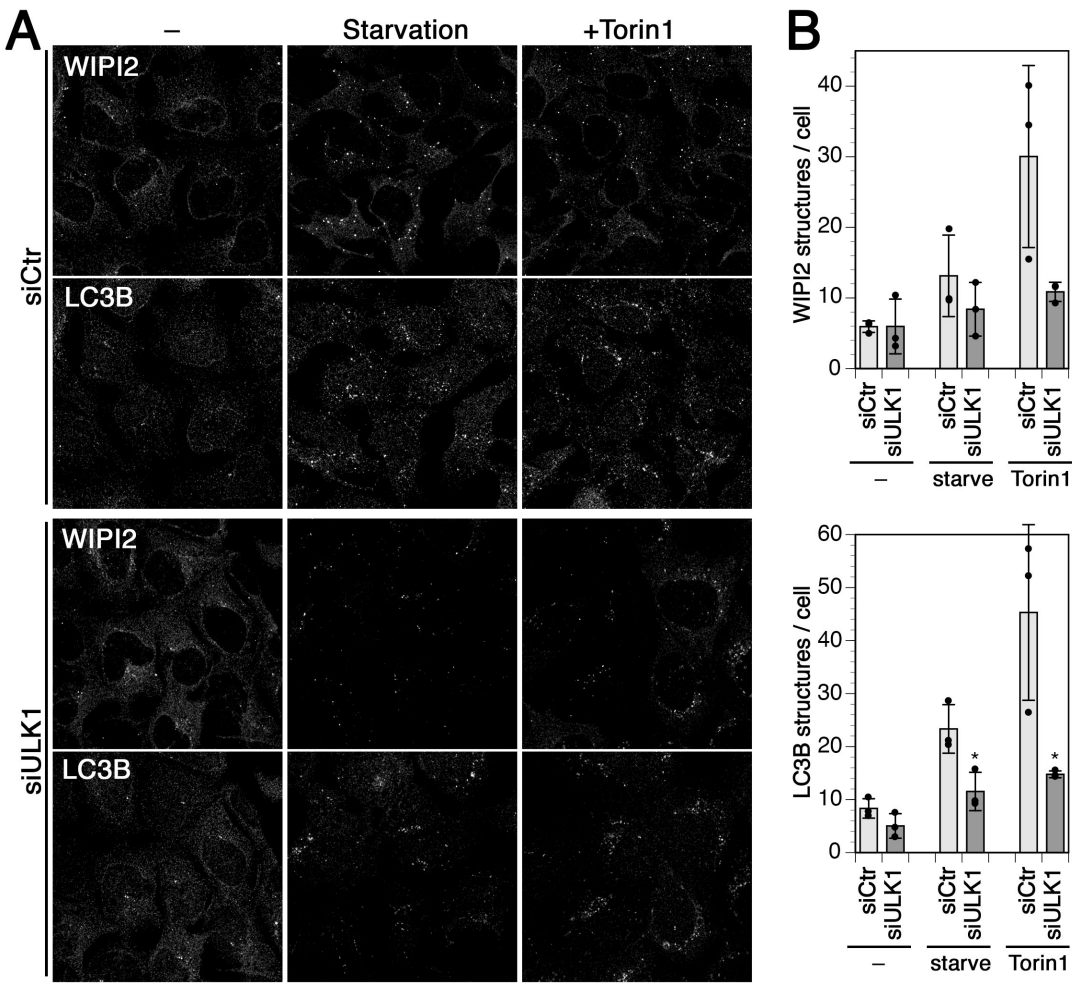

Suppl. Figure S2. ULK1 knockdown inhibits starvation- and Torin1-induced autophagy.
A: HEK293A cells were transfected with nontargeting siRNA (siCtr) or siRNAs silencing ULK1 for 72 h, and treated without (–) or with 250 nM Torin1 for 3 h, or starved in HBSS for 150 min. Cells were fixed and immunostained for endogenous WIPI2 and LC3B. Bar, 10 µm.
B and C: WIPI2 (B) of LC3B puncta per cell (C) were quantified for each condition (mean and standard deviation of three independent experiments; two-tailed Student's t test: *$p < 0.05$).

bioRxiv preprint doi: https://doi.org/10.1101/2020.09.01.277764; this version posted September 1, 2020. The copyright holder for this preprint (which was not certified by peer review) is the author/funder. All rights reserved. No reuse allowed without permission.

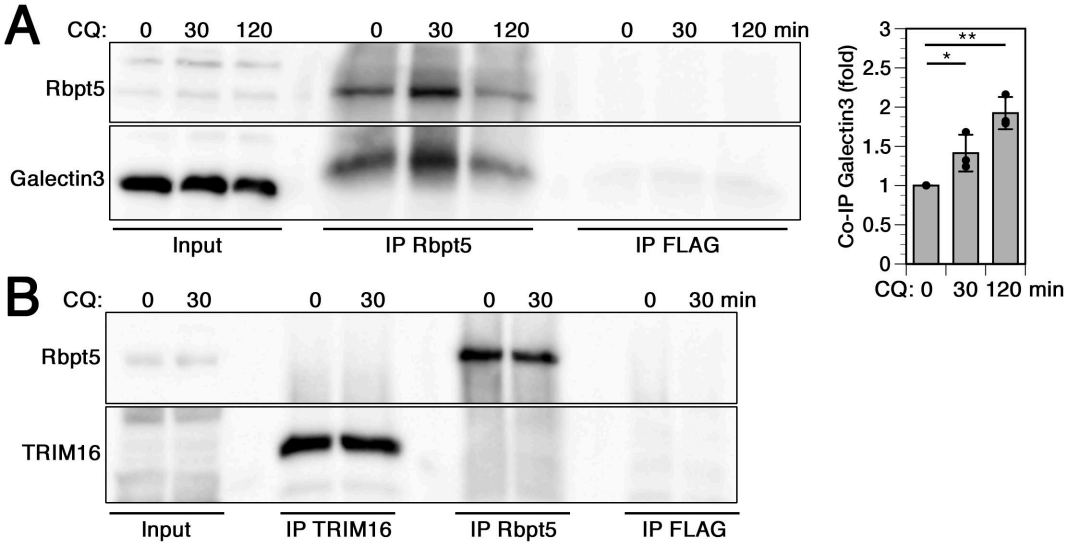

Suppl. Figure S3. Galectin3, but not to TRIM16, is co-immunoprecipitated with Rabaptin5.
A: Lysates of HeLa cells treated with 60 µM chloroquine for 0, 30, or 120 min were immunoprecipitated with anti-Rabaptin5 (IP: Rbpt5) or, as a control, with anti-FLAG antibodies (IP FLAG). Immunoprecipitates and input lysates (10%) were immunoblotted for Rabaptin5 and galcetin3. Signals were quantified and the ratios of galectin3/Rabaptin5 normalized to that without (0 min) chloroquine treatment are shown (mean and standard deviation of three independent experiments; two-tailed Student's t test: *$p < 0.05$; **$p<0.01$).
B: Lysates of HeLa cells treated with 60 µM chloroquine for 0 or 30 min were immunoprecipitated with anti-TRIM16 (IP TRIM16), anti-Rabaptin5 (IP Rbpt5), or anti-FLAG antibodies (IP FLAG). Immunoprecipitates and input lysates (10%) were immunoblotted for Rabaptin5 and TRIM16.

bioRxiv preprint doi: https://doi.org/10.1101/2020.09.01.277764; this version posted September 1, 2020. The copyright holder for this preprint (which was not certified by peer review) is the author/funder. All rights reserved. No reuse allowed without permission.

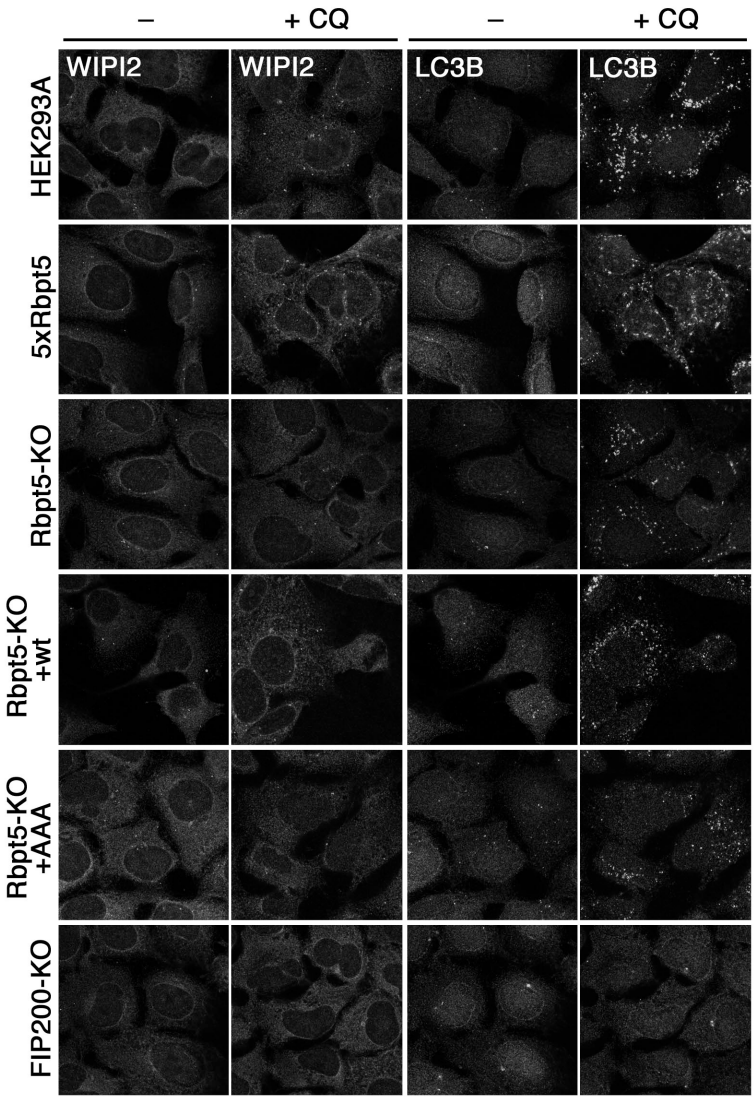

Suppl. Figure S4. Chloroquine-induced endosomal autophagy depends on Rabaptin5 and its ATG16L1 binding motif.

Wild-type HEK293A cells, HEK^{+Rbpt5} cells stably overexpressing Rabaptin5, Rabaptin5-knockout cells without (Rbpt5-KO) or with stable re-expression of wild-type (Rbpt5-KO+wt) or AAA-mutant Rabaptin5 (Rbpt5-KO+AAA), and FIP200-knockout cells were incubated without (–CQ) or with 60 µM chloroquine for 150 min (+CQ), and analyzed by immunofluorescence microscopy for WIPI2 or LC3B. Bar, 10 µm. Quantitation of WIPI2 and LC3B puncta per cell is shown in Figure 7B and C.

bioRxiv preprint doi: https://doi.org/10.1101/2020.09.01.277764; this version posted September 1, 2020. The copyright holder for this preprint (which was not certified by peer review) is the author/funder. All rights reserved. No reuse allowed without permission.

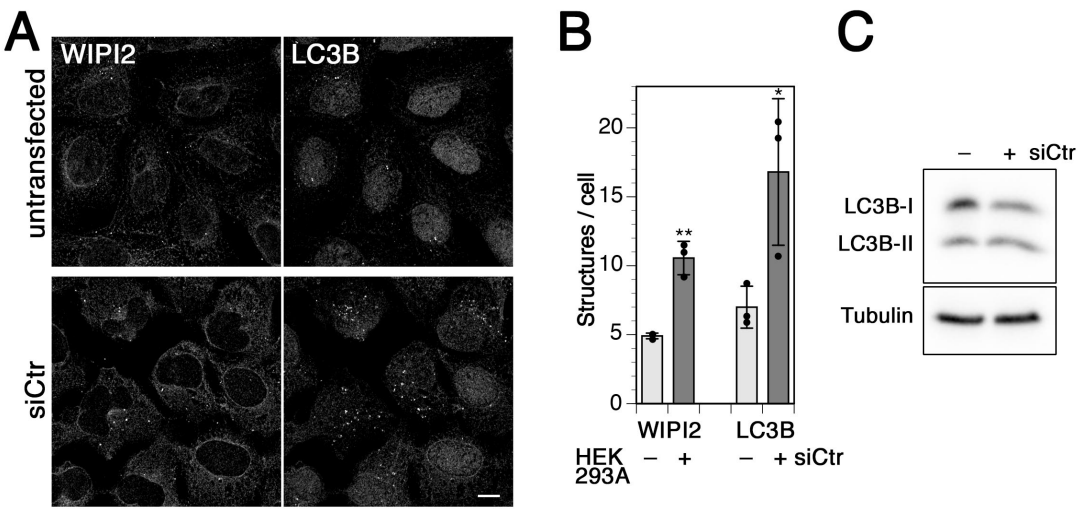

Suppl. Figure S5. siRNA transfection increases basal autophagy.
A: HEK293A cells were transfected with nontargeting siRNA (siCtr) for 72 h or not treated. Cells were fixed and immunostained for endogenous WIPI2 and LC3B. Bar, 10 µm.
B: WIPI2 and LC3B puncta per cell were quantified (mean and standard deviation of three independent experiments; two-tailed Student's t test: *$p < 0.05$, **$p < 0.01$).
C: Lipidated and non-lipidated LC3B (I and II, resp.) from lysates of HEK293A cells transfected or not with nontargeting siCtr were assayed by immunoblot anlysis.

bioRxiv preprint doi: https://doi.org/10.1101/2020.09.01.277764; this version posted September 1, 2020. The copyright holder for this preprint (which was not certified by peer review) is the author/funder. All rights reserved. No reuse allowed without permission.

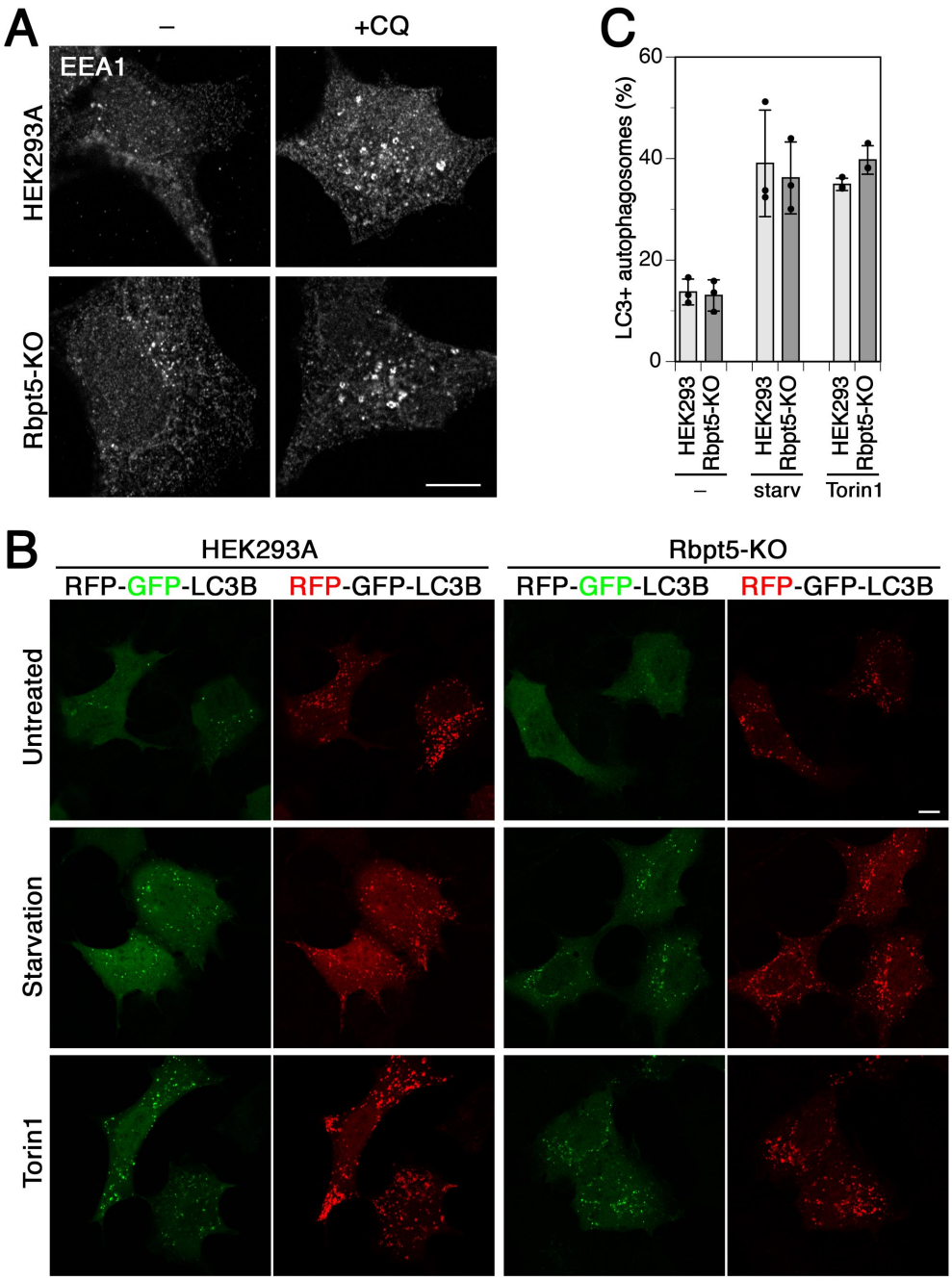

Suppl. Figure S6. Rabaptin5 knockout does not affect sensitivity of early endosomes to chloroquine or autophagic flux.

A: Treatment of HEK293A and Rabaptin5-KO cells with 60 µM chloroquine for 30min similarly leads to swelling of early endosomes positive for EEA1 as detected by immunofluorescence.

B: HEK293A cells and Rabaptin5-KO cells were transduced to express tandem fluorescent RFP-GFP-LC3, starved in HBSS or treated with 250 nM Torin1 for 3 h, fixed and subjected to fluorescnet microscopy. Images for at least 16 cells per sample were quantified.

C: The number of autophagosomes (GFP+/RFP+) and autolysosomes (GFP /RFP+) LC3 puncta were counted and autophagosomes plotted as a percentage of the total (mean and standard deviation of three independent experiments).

bioRxiv preprint doi: https://doi.org/10.1101/2020.09.01.277764; this version posted September 1, 2020. The copyright holder for this preprint (which was not certified by peer review) is the author/funder. All rights reserved. No reuse allowed without permission.

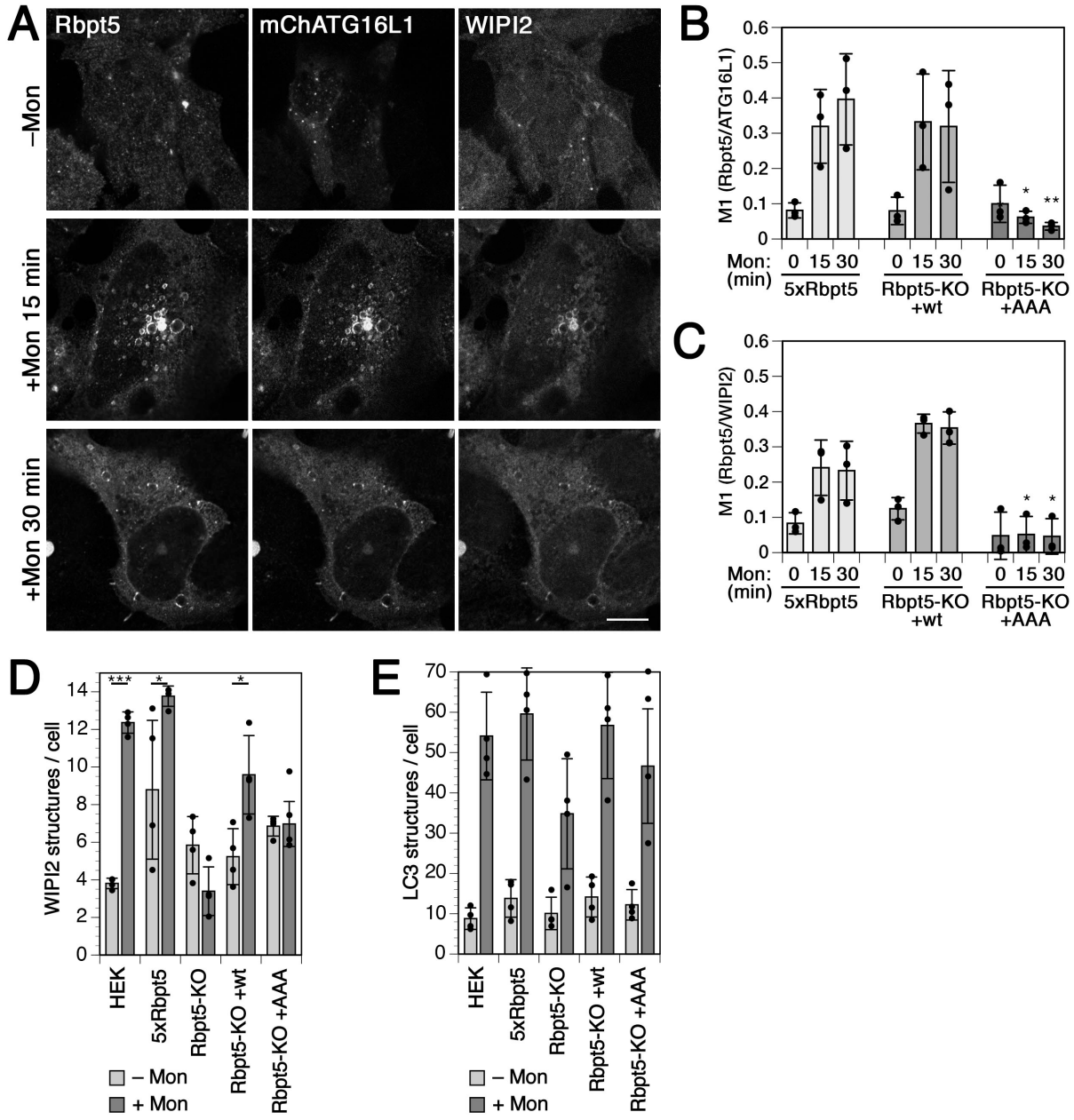

Suppl. Figure S7. Monensin induces endosomal autophagy dependent on Rabaptin5 and ATG16L1 binding just like chloroquine.

A: HEK^{+Rbpt5} cells, 24 h after transfection with mCherry-ATG16L1, were treated with 100 µM monensin for 0, 15 and 30 min and stained for Rabaptin5,WIPI2, and mCherry-ATG16L1 to assess their colocalization on swollen early endosomes. Bar, 10 µm.

B and **C**: Mander's colocalization coefficients were determined, showing the fraction of Rabaptin5-positive structures also positive for mCherry-ATG16L1 (B) or for WIPI2 (C) (mean and standard deviation of three independent experiments, quantifying ~40 cells for each sample; two-tailed Student's t test for Rbpt5-KO+AAA vs. HEK^{+Rbpt5} cells : *$p < 0.05$, **$p < 0.01$).

D and **E**: Wild-type HEK293A cells, HEK^{+Rbpt5} cells, and Rabaptin5-knockout cells without (Rbpt5-KO) or with stable re-expression of wild-type (Rbpt5-KO+wt) or AAA-mutant Rabaptin5 (Rbpt5-KO+AAA) were treated without (–Mon) or with 100 µM monensin for 30 min (+Mon), and analyzed by immunofluorescence microscopy for WIPI2 or LC3B. WIPI2 (D) of LC3B (E) puncta per cell were

bioRxiv preprint doi: https://doi.org/10.1101/2020.09.01.277764; this version posted September 1, 2020. The copyright holder for this preprint (which was not certified by peer review) is the author/funder. All rights reserved. No reuse allowed without permission.

quantified for each condition (mean and standard deviation of four independent experiments; two-tailed Student's t test: *$p < 0.05$, **$p < 0.01$, ***$p<0.001$).

bioRxiv preprint doi: https://doi.org/10.1101/2020.09.01.277764; this version posted September 1, 2020. The copyright holder for this preprint (which was not certified by peer review) is the author/funder. All rights reserved. No reuse allowed without permission.

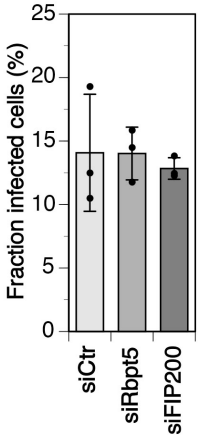

Suppl. Figure S8. Infection efficiency of Salmonella is not affected upon silencing of Rabaptin5 or FIP200.

HeLa cells were transfected with nontargeting siRNA (siCtr) or siRNAs silencing Rabaptin5 (siRbpt5) or FIP200 (siFIP200) for 72 h, infected with *Salmonella* expressing GFP and washed as in Figure 8A and immediately fixed for fluorescence microscopy and stained with anti-transferrin receptor and anti-LC3B. Z-stacks for >5'000cells/sample were acquired and analyzed in Fiji to determine the fraction of infected cells (mean and standard deviation of three independent experiments). The average number of bacteria per infected cell was identical (2.16, 2.11, and 2.12 bacteria per cell transfected with siCtr, siRbpt5, and siFIP200, resp.).

bioRxiv preprint doi: https://doi.org/10.1101/2020.09.01.277764; this version posted September 1, 2020. The copyright holder for this preprint (which was not certified by peer review) is the author/funder. All rights reserved. No reuse allowed without permission.

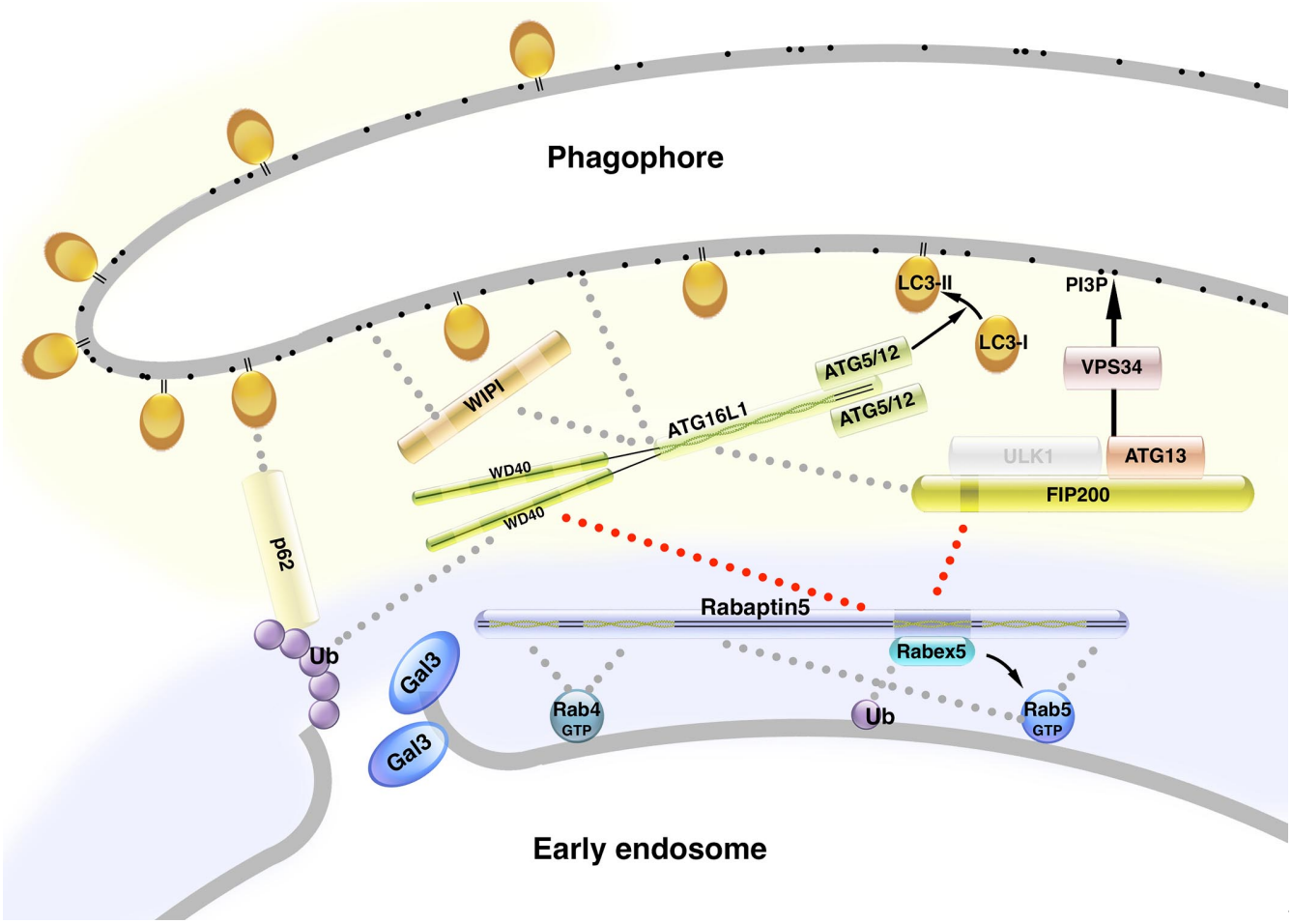

Suppl. Figure S9. Rabaptin5 connects damaged endosomal membranes to the autophagic machinery.

Schematic model of early endosomes positive for the complex of Rabaptin5 (interacting with Rab4 and Rab5) and Rabex5 (binding to mono-ubiquitinated receptors and activating Rab5 by GDP/GTP exchange). Upon rupture by treatment with chloroquine or monensin, lumenal glycoproteins are exposed that recruit cytosolic galectins and are poly-ubiquitinated. Rabaptin5 connects to the autophagic machinery network by binding to FIP200 and the WD domains of ATG16L1 activating phagophore recruitment and expansion with activation of LC3-I to lipidated LC3-II. Binding interactions are illustrated by dotted lines in gray and, for the novel ones discovered in this study, in red. The interactomes of early endosomes and autophagy are highlighted by blue and yellow backgrounds, respectively. Ub, ubiquitin; black dots, PI3P. ULK1 is grayed out, since it is not required in the process.